ARMY RESEARCH LABORATORY

An Examination of the Feasibility of Ultrasonic Communications Links

by David Tofsted, Sean O'Brien, Sean D'Arcy, Edward Creegan, and Scott Elliott

ARL-TR-5200 **June 2010**

Approved for public release; distribution is unlimited.

NOTICES

Disclaimers

The findings in this report are not to be construed as an official Department of the Army position unless so designated by other authorized documents.

Citation of manufacturer's or trade names does not constitute an official endorsement or approval of the use thereof.

Destroy this report when it is no longer needed. Do not return it to the originator.

Army Research Laboratory
White Sands Missile Range, NM 88002-5513

ARL-TR-5200 **June 2010**

An Examination of the Feasibility of Ultrasonic Communications Links

David Tofsted, Sean O'Brien, Sean D'Arcy,
Edward Creegan, and Scott Elliott
Computational and Information Sciences Directorate, ARL

Approved for public release; distribution is unlimited.

REPORT DOCUMENTATION PAGE	Form Approved OMB No. 0704-0188

Public reporting burden for this collection of information is estimated to average 1 hour per response, including the time for reviewing instructions, searching existing data sources, gathering and maintaining the data needed, and completing and reviewing the collection information. Send comments regarding this burden estimate or any other aspect of this collection of information, including suggestions for reducing the burden, to Department of Defense, Washington Headquarters Services, Directorate for Information Operations and Reports (0704-0188), 1215 Jefferson Davis Highway, Suite 1204, Arlington, VA 22202-4302. Respondents should be aware that notwithstanding any other provision of law, no person shall be subject to any penalty for failing to comply with a collection of information if it does not display a currently valid OMB control number.
PLEASE DO NOT RETURN YOUR FORM TO THE ABOVE ADDRESS.

1. REPORT DATE *(DD-MM-YYYY)*	2. REPORT TYPE	3. DATES COVERED (From - To)
June 2010	Final	September–November 2009

4. TITLE AND SUBTITLE
An Examination of the Feasibility of Ultrasonic Communications Links

5a. CONTRACT NUMBER

5b. GRANT NUMBER

5c. PROGRAM ELEMENT NUMBER

6. AUTHOR(S)
David Tofsted, Sean D'Arcy, Edward Creegan, and Scott Elliott

5d. PROJECT NUMBER

5e. TASK NUMBER

5f. WORK UNIT NUMBER

7. PERFORMING ORGANIZATION NAME(S) AND ADDRESS(ES)
U.S. Army Research Laboratory
Computational and Information Sciences Directorate
Battlefield Environment Division (ATTN: RDRL-CIE-D)
White Sands Missile Range, NM 88002-5501

8. PERFORMING ORGANIZATION REPORT NUMBER
ARL-TR-5200

9. SPONSORING/MONITORING AGENCY NAME(S) AND ADDRESS(ES)

10. SPONSOR/MONITOR'S ACRONYM(S)

11. SPONSOR/MONITOR'S REPORT NUMBER(S)

12. DISTRIBUTION/AVAILABILITY STATEMENT
Approved for public release; distribution is unlimited.

13. SUPPLEMENTARY NOTES

14. ABSTRACT
A study is performed to consider the feasibility of using the ultrasonic band just above the normal adult audio frequency range (20–25 kHz) for low data rate signaling. In this band several features of interest are explored and a potential application (Identification Friend-or-Foe [IFF]) is highlighted. A key finding is that the data transmission rate is restricted in the presence of multipathing effects. Data transmission rates in the 300-baud range are possible when Rician noise statistics dominate. For non-line-of-sight cases when Rayleigh statistics dominate, a data link may not be possible. However, in the presence of a dominant reflecting path data may be transmittable, but at greatly reduced rates, due to multipathing. To study the potential of this technology a series of measurements were performed to determine signal losses with range, angular emission properties of a series of horns as a function of frequency, and Amplitude Modulation (AM) and Frequency Modulation (FM) data encoding methods.

15. SUBJECT TERMS
ultrasonic propagation, acoustics, multipathing, bit-error-rate

16. SECURITY CLASSIFICATION OF:			17. LIMITATION OF ABSTRACT	18. NUMBER OF PAGES	19a. NAME OF RESPONSIBLE PERSON
a. REPORT	b. ABSTRACT	c. THIS PAGE			David Tofsted
Unclassified	Unclassified	Unclassified	UU	62	19b. TELEPHONE NUMBER (*Include area code*) (575) 678-8547

Standard Form 298 (Rev. 8/98)
Prescribed by ANSI Std. Z39.18

Contents

List of Figures

List of Tables

Executive Summary

This report documents a feasibility study performed at White Sands Missile Range (WSMR), NM, in the fall of 2009. This study addressed the issue of the capabilities and limitations associated with ultrasonic acoustic data communications. There exist a number of relevant Army field problems that could potentially benefit from such systems, since many distributed systems such as intelligent minefields or arrays of meteorological sensors could be more easily emplaced if they did not require wires to connect to one another.

The readiest alternative is, of course, the electromagnetic spectrum. However, this spectrum is already widely used and easily intercepted, possibly compromising the safety or security of a network using this technology. Infrared communications are likewise easily detected.

The advantage of ultrasonic acoustic transmissions is that they operate at frequencies that are significantly attenuated by the atmosphere and therefore provide a stealth advantage. Ultrasonic signals are naturally undetectable by a human without instrumentation. Second, due to high attenuation rates, ultrasonic signals can only be detected within close proximity to an emitter. They are typically undetectable beyond approximately 100 m of a source. Also, because the air is the information carrier, signals can be broadcast to multiple sensors simultaneously, like radio. Low data rate signals can also be consolidated for rebroadcast from a single receive point via a single Radio Frequency (RF) uplink, avoiding bandwidth limitations. Hence, for a localized sensor network, as long as the needed bandwidth is not too high, an ultrasonic network could provide a useful option.

A series of hardware devices, software tools, and computer algorithms were developed to facilitate measurements and testing that allow an objective assessment of the feasibility for ultrasonic data communication in a field environment. The foundation for the basic ultrasonic communications system used in this investigation is based on the Laboratory Virtual Instrument Engineering Workbench (LabVIEW) software package and hardware interface modules. One of the metrics used in this study is the integrity of binary data that are ultrasonically broadcast from a transmitter to a downrange receiver. For this purpose, data strings were translated into a series of bits and transmitted using Amplitude Modulation (AM) and Frequency Modulation (FM) implementations. Both the transmitter modulation and receiver demodulation were controlled by the LabVIEW system implementation. As described in our report, early results focused our major interest on FM modulation using a binary Frequency Shift Keyed (FSK) system.

A series of four emitting horns were employed to examine the role played by transmission patterns in the efficiency of data conveyance and energy propagation. A parabolic dish was found to concentrate the most energy in the forward direction, but for the purpose of broadcasting digital data signals, a wide-angle rectangular horn was deemed to be the most

versatile form factor, and was selected as the most appropriate for extended testing. On the receive side a high sensitivity uniform responsivity microphone was used. Using these components, it was found that for direct transmissions at relatively short ranges, i.e., 5–10 m, a bit-transmission-rate of 400 baud was obtainable.

However, significant reduction in fidelity is associated with multipathing geometries between a transmitter and receiver pair. We found that reflections from surfaces frequently confused our basic system, requiring the bit-transmission rate to be reduced considerably.

We found that by reducing the baud rate to around five bits per second the effects of multipathing can be reversed from detrimental to a geometric advantage, since the addition of reflected trajectories permits signals to be transmitted over non-line-of-sight paths, effectively propagating around corners. Such data rates would, of course, not be useful for propagating significant amounts of information such as might be required for meteorological or smart mine applications. However, such signals could prove useful in an Identification Friend-or-Foe (IFF) application where relatively few bytes of data could yield information necessary to verify the identity of nearby friendly forces. As an example, this technology could be useful when ground assault forces are advancing into an urban setting from multiple access points.

We have thus documented what we believe to be an initial capability to perform such low data rate tasks for an urban scenario involving building wall reflections, or longer range clear-path data propagation. Further refinements are expected to be necessary to properly exploit such a capability, to include a more extensive study of varying frequency transmission modes, refinement of the signal discrimination methodology, the handling of noise sources, and (particularly) wind variability effects that shift propagated frequencies.

1. Introduction

For over 40 years the U.S. Army Research Laboratory's (ARL) Battlefield Environment Division (BED) (formerly the U.S. Army Atmospheric Sciences Laboratory) has provided models, measurements, and effects related models predicting the impacts of near-earth atmospheric characteristics on U.S. Army systems and soldiers. Development of models to characterize problems such as the propagation of electromagnetic energy through battlefield dust, explosive clouds, background aerosols, and other aerosol contaminants have been a critical element of the program. Another component of this program was an active effort to assess the impacts of optical turbulence on developmental laser and imaging systems. Indeed, the role of turbulence (both thermal and kinematic) has been crucial in many aspects of these studies. Optical turbulence can have a highly deleterious effect on the propagation of coherent energy. Turbulence also manifests itself in its influence on the transport and diffusion of smoke and other battlefield obscurants, generating fluctuations in aerosol density. Hence, the measurement of turbulence, both optical and mechanical, has been an ongoing interest.

1.1 Prior ARL Atmospheric Turbulence and Acoustics Efforts

Optical devices known as scintillometers are among the sensors used to characterize turbulence levels. However, scintillometers only sense integrated path optical turbulence. For the past decade, ARL has increasingly relied on ultrasonic acoustic anemometers, such as the R. M. Young series 81000 three-component sonic anemometers commonly used for quasi-point high frequency (20 Hz) wind speed and direction measurements. These devices measure each of the orthogonal (U, V, W) wind speed components based on the difference between the crossing times of two oppositely-directed ultrasonic pulses that are passed through a sampled air gap over a very short time span. At the same time, these devices use a calculation of the mean temperature to correct for temperature fluctuations during measurement. This temperature measurement also facilitates a rapid sensing of point thermal fluctuations.

Also, historically, ARL has supported the general characterization of atmospheric conditions during field experiments. A common method used in the remote sensing of lower level winds has been Sonic Detection And Ranging (SODAR). SODAR equipment generates atmospheric profiles of wind and thermal fluctuations using Doppler scattering from density fluctuations. This SODAR instrumentation operates on the principle of signal processing and mapping of the acoustic energy backscattered from discrete atmospheric gradients of temperature and/or winds. In particular, SODAR energy will scatter at the level of thermal inversions in the atmosphere at night. As an example of an ARL product developed with this technology, the Meteorological Measuring Set (MMS) AN/TMQ-41 Atmospheric Profiler prototype developed by BED incorporated a Radio Acoustic Sounding System (RASS) for low-level virtual temperature profile measurements. This system provides the U.S. Army field artillery with a remote lower-

echelon meteorological measurement capability which would take the meteorological balloon with its associated logistics off the battlefield. The implementation of the MMS RASS involved the incorporation of three different acoustic sounding sub-systems, all of which operated in the mid-audible range of a few kiloHertz (Cogan et al., 1997). (These instruments were large trailer-mounted items weighing several hundred pounds each.)

The SODAR and RASS units that ARL evaluated emitted high amplitude acoustic energy so that the pulsed signals generated would be powerful enough to meet the requirements for measurements at maximized altitudes. By operating in the audible range they took advantage of the relatively low molecular attenuation rates of acoustic energy at low frequencies. This allowed for increased altitude performance capability. However, this required a tradeoff–greater range for greater weight.

1.2 Motivation for Current Ultrasonic Propagation Research

Revisiting some of these concepts, it is apparent that not all sound frequency domains have been fully exploited. In particular, various applications for the ultrasonic spectrum may be feasible. One example is a technique for studying raindrop size distributions and rain rates using a bistatic ultrasonic backscatter system based on the variable Doppler shift due to the dependence of terminal velocity on droplet size (Bradley and Webb, 2001).

It may also be possible to sense wind profiles using ultrasonic devices that detect energy scattered from boundary layer turbulence. Though the ranges of such instruments would be necessarily shorter, in several applications short ranges may be advantageous. The shorter wavelength of ultrasonic radiation would also permit reductions in size and weight of such instrumentation and support greater granularity in any measurements made.

However, the application considered in the present study is the potential for ultrasonic communications capabilities. With the proliferation of radio signals at nearly every frequency, plus the ability to jam or remotely monitor radio equipment, an ultrasonic system that does not rely on radio could prove useful. While such a system would operate, necessarily, at short ranges, any attempt to jam it would also need to be performed at short range. For a system such as a smart minefield, any system that attempted to jam an ultrasonic communications system operated by the field would itself be detectable as an intrusion, alerting the field.

Another possible outdoor application would be in a weather reporting network of interconnected meteorological (met) sensors. Such a net would not need to operate in a stealth mode, because it would primarily be used for information purposes. However, from the standpoint of RF bandwidth, the sensors of such a network could be set up with clear lines of sight connecting adjacent sensors, permitting high data transmission rates, yet avoiding the assignment of separate RF frequencies to each sensor and avoiding the interference possible between adjacent IR links.

1.3 Prior Art

While the field of ultrasonic communications is not extensive, several research programs have studied various aspects of the problem. Haynes et al. (2000) considered various fundamental aspects of such systems. They developed both digitally controlled systems and digital/analog hybrid prototypes. Their initial efforts were conducted in 1993, focusing on frequency modulation methods designed to modulate voice and music signals to ultrasonic frequencies, propagate these signals through air, and demodulate these signals through receiver hardware. Initially this equipment consisted primarily of phase-lock-loop and voltage-to-frequency conversion hardware. This work was patented in 1996 (Akerman et al., 1996). A follow-up program was conducted in 1998–1999 that transitioned their hardware to largely computer controlled (Laboratory virtual Instrument Engineering Workbench [LabVIEW]) modulation methods. This project studied propagation of ultrasonic signals through water and air filled pipes. These efforts followed an approach similar to those reported here: digital methods were used to communicate symbols based on the American Standard Code for Information Interchange (ASCII) character codes. Frequency modulation methods were employed to avoid variations in signal amplitude. This technique suppresses audible detection of breaks between transmitted data bits. Their use of pipes to direct sound waves is an effective methodology for eliminating the deleterious impacts of multipathing on inter-symbol interference.

Holm (2005) reported on his analysis of the channel capacity of an indoor ultrasonic positioning system. This system consisted of tagging hospital equipment with ultrasonic emitters that communicated with in-room receivers. Equipment transmitted its identity when moved. Holm analyzed the bit data transmission rate possible for this system in the presence of interfering noise sources, Doppler shift effects, and reverberations (presumably due to multipathing). His analysis relied on Shannon (1948) information theory and considered a Frequency Shift Keying (FSK) modulation scheme. For this case he found that the maximum channel efficiency should approach 0.025 bits per second per Hz. He observed, however, that this efficiency is less than is achieved by human speech and by certain systems of whistled languages (Busnel and Classe, 1976). Hence he concluded that advanced modulation techniques should exceed the above channel efficiency. For ultrasonic signals in the 20–25-kHz range using the above result we would expect to achieve 500–625-bits per second (baud) data rates using FSK modulation.

Li et al. (2008) approached the problem of indoor ultrasonic communications by considering a higher frequency regime (above 100 kHz). Presumably higher data rates could be achieved by increasing the bandwidth. However, from the perspective of our research, higher frequencies reduce range capability due to increased atmospheric attenuation. However, this paper contains a much more complete review of the research field. They cite Heard (1983), who appears to have been the earliest researcher in this area. He employed a high powered amplitude modulation to generate signals. They also cite a patent by Zurek et al. (2002) that used an ultrasonic system to operate a wireless computer mouse.

One might wonder that there are numerous ultrasonic conferences, yet Li et al., cited so few relevant documents. The answer is that our application area and the ultrasound field are both designated under the umbrella term of ultrasonics. And though the technology of ultrasound is extensive, the frequency regime at which this equipment operates (200–300 kHz) limits its application to our research. Ultrasound propagates primarily over short ranges within variable body media. Atmospheric propagation applications involve different attenuation rates, scattering due to temperature and wind turbulence, and variable signal absorption dependent on atmospheric state.

Due to these factors, and especially due to turbulent scattering, most ultrasonic communications systems have been designed for indoor use only. The focus of our research is for both indoor and outdoor use, consistent with Army applications. Section 2 considers modeling of this propagation environment.

1.4 Program of Investigation

Two approaches were followed for determining the characteristics and limitations of ultrasonic data communication networks. As a basic first approach, we measured the levels of sound propagated to different ranges under varying propagation conditions for a simple ultrasonic emitter and receiver pair. In more sophisticated second approach, a simple communication system consisting of a single set of ultrasonic emitter and receiver devices was devised and exercised to test the capability for transmitting information over different communications link path geometries.

Several test site venues were used for early ultrasonic propagation experiments prior to establishing a more permanent site for these measurements. The first tests were performed by propagating ultrasonic energy down a hallway path in the basement of building 1622 at White Sands Missile Range (WSMR). The goal of these first tests was to study the sound level range dependence of a battery powered ultrasonic sound generator. However, these tests revealed the extreme sensitivity of ultrasound to reflections from walls in enclosed spaces such as the tunnel-like hallway. These indoor tests produced inconsistent results and were moved outdoors to eliminate spurious reflections from hard walls.

Thus, a second venue for the ultrasonic propagation tests was in a flat, open, dirt-covered area behind building 1622. Results for ranges up to 16 m were measured. Here too, inconsistent variations in received acoustic intensity versus range (as measured by a Sound Pressure Level [SPL] meter) raised questions concerning the relative impacts of SPL losses due to molecular signal attenuation effects, atmospheric scattering due to turbulence, and the effects of multipathing. In these first outdoor experiments, the emitter used was not focused in any way, so that the close proximity of the ground to the acoustic path could well have enhanced multipath contamination of the direct-path signal.

The inconclusive nature of these first two indoor/outdoor tests near building 1622 led us to relocate to a more controllable environment at the building 19472 compound south of the main base area at WSMR. The advantages of this site are its remote location, where sound-based tests will not interfere with other range or ARL operations, as well as the ability to leave the test range in a particular configuration indefinitely. In particular, a scaffold was erected at a location on this site that permits the use of a focused emitter on a slant-path that substantially reduces the influences of ground reflections. The facility layout, equipment, safety procedures, and the testing schedule adopted are described in section 3.

With this new facility configuration, experiments were then designed to characterize the performance of ultrasonic communication proof-of-concept systems, with respect to acoustic propagation in general and to ultrasonic FSK coded propagation in particular. The observed effects of atmospheric attenuation, wind conditions, and multipath interference on coded signal propagation and fidelity are discussed below. The LabVIEW-based software developed to provide Amplitude Modulation (AM) and FSK modulation and demodulation of propagated SPL measurements are described in section 4. An analysis of the AM and Frequency Modulation (FM) binary-coded acoustic signals of ultrasonic, and audible, frequencies generated and received are evaluated in section 5. Section 6 also includes a discussion of the salient features and limitations of such systems under varying conditions. Section 7 then presents conclusions.

2. Semi-Empirical Ultrasonic Absorption and Scattering Models and Early Experimental Findings

The literature concerning models of ultrasonic atmospheric absorption and scattering from atmospheric turbulence has a history extending back several decades. The acoustic scattering and absorption model described by Shamanaeva and Burkatovskaya (2004) is a convenient distillation of various prior formulations. Acoustic energy absorption is divided primarily into classical and molecular absorption effects. Models of these influences derived from earlier publications by Neff (1975), Sutherland (1968), and even earlier works cited by Sutherland. Formulations for scattering of acoustic energy from temperature and wind turbulence used in this analysis were derived from Shamanaeva (1983) and Baikalova et al. (1988). In this section, we shall summarize these models and then compare these with some of data collected during our earliest outdoor experimental results.

2.1 Acoustic Absorption and Scattering Cross Sections

We first consider a simplified theory for atmospheric absorption and scattering cross sections for ultrasonic energy. Of course, our interest in both these factors is not merely academic. We intend (ultimately, for some applications) to attempt to measure wind scattering of acoustic

pulses. Likewise, molecular absorption of ultrasonic energy will strongly affect the level of path losses in virtually all potential applications.

In this instance, we are only interested in direct propagation between a source and a receiver (in the absence of reflections). Therefore, the received to transmitted power ratio may be expressed as

$$P_r / P_t = Tr\, R_0^2 / R^2 , \tag{1}$$

where the factor Tr is the path transmission, R is the range, and R_0 is the baseline range (nominally 1 m) at which the initial power level is measured. The transmission factor encapsulates various loss mechanisms, and can be further expressed as

$$Tr = \exp\left[-(\alpha_a + \alpha_t)(R - R_0)\right], \tag{2}$$

where α_a and α_t are the absorption and turbulent scattering coefficients [m^{-1}], respectively.

Kaye and Laby (2009), provide tabular results for the molecular attenuation coefficients, based on the ISO 9613-1 standard (1993). Representative values are given in table 1. These data reflect an interesting property of the absorption of acoustic energy which depends on the interactions between the acoustic energy, atmospheric density, and molecular absorption resonance frequencies.

Table 1. Attenuation of sound in air (dB km^{-1}).

Frequency (kHz)	**Relative Humidity %**								
	10	20	30	40	50	60	70	80	90
4	110	75	49	36	30	26	23	21	20
8	180	220	170	130	110	89	78	69	63
12.5	210	360	340	280	240	200	180	160	140
16	230	430	470	420	360	320	280	250	230
20	260	510	600	580	520	470	420	380	350
25	300	580	740	770	730	680	620	570	520

An algorithm modified by Desart (2004) calculates these coefficients using a relatively simple algorithm. A closer consideration of variations in humidity (which will be given in following

subsection) would be useful in future measurements, because model results indicate that even under extremely dry conditions, 2–3-dB losses would be experienced over 10 m propagation ranges. Our measurements have all been performed on relatively dry days that are characteristic of New Mexico climate, where relative humidity levels of 20% or less are the norm.

We now examine Ishimaru's approach for predicting the impacts of turbulent scattering. He defines the acoustic scattering cross section per unit volume (Ishimaru, 1978, pg. 344, equations [16–58]) as,

$$\alpha_t(\theta) = 2\pi\, k^4 \cos^2(\theta)\, \Phi_n(\kappa_s), \tag{3}$$

where $\kappa_s = 2k\sin(\theta/2)$ is a sampling wavenumber, θ is the scattering angle between the direction of the incident sound wave and the scattered wave, and $k = 2\pi/\lambda$ is the radiation wavenumber.

$\Phi_n(\kappa_s)$ is the turbulence spectral density given by

$$\Phi_n(\kappa_s) = \cos^2(\theta/2)\,\Phi_V(\kappa_s)/c_0^2 + \Phi_T(\kappa_s)/4T_0^2, \tag{4}$$

where $\Phi_V(\kappa_s)$ and $\Phi_T(\kappa_s)$ are the spectral densities of the velocity field and the temperature field, respectively, c_0 is the mean speed of sound [m/s], T_0 is the mean temperature [K], and the spectra are given by,

$$\Phi_V(\kappa_s) = 0.061 C_V^2\, \kappa_s^{-11/3} \text{ and } \Phi_T(\kappa_s) = 0.033 C_T^2\, \kappa_s^{-11/3}, \tag{5}$$

where C_V^2 and C_T^2 are the structure parameters of velocity and temperature, respectively. Ishimaru lists typical ranges for these parameters as $10^{-4} < C_V^2 < 1$ [(m/s)^2/m$^{2/3}$] and $10^{-3} < C_T^2 < 10^{-1}$ [deg^2/m$^{2/3}$].

These spectral forms, however are only valid for spatial frequencies occupying the inertial subrange: $1/L_o < \kappa_s < 1/\ell_o$, where L_o and ℓ_o are the inner and outer scales of turbulence, respectively.

For a somewhat more quantitative range estimate for C_T^2, its relationship to the refractive index structure parameter, C_n^2, can be considered. It is well known that typical values for C_n^2 at heights within the first 20–40 m of the surface generally range between 10^{-15}–10^{-13} m$^{-2/3}$. One can estimate the value of C_T^2 based on the expression, $C_T^2 = C_n^2\, T_0^4 / A^2\, P^2$, where $A = 79\times10^{-6}$ K/mbar, and P is the atmospheric pressure in millibars. Using standard pressure and temperature values (1013-mbar, 288-K), C_T^2 ranges between 0.00107 and 0.107. So the low value obtained is under weak turbulence, and the high value used is under typical daytime conditions at WSMR. We also note that the maximum scattering due to wind fluctuations occurs in the forward direction, while there is zero contribution due to wind in the backscattering

direction. Also note that Ishimaru's (1978) form cannot be correct in the exact forward scattering direction since the $\sin(\theta/2)$ dependence in κ_s when introduced into either spectrum produces an approximate $\theta^{-11/3}$ divergent behavior at zero scattering angle. We attempted to observe results in the forward scattering direction, so the failure of the Ishimaru (1978) functional form in this domain is a matter of some concern. Fortunately, other models of a semi-empirical nature (e.g., Shamanaeva, 2004) are available to estimate the forward scattering effects at ultrasonic frequencies. Shamanaeva's model (which is based on a series of earlier results) will now be presented in the next subsection. Unfortunately, Shamanaeva used a different pair of governing variables: acoustic frequency, *f*, and wavelength, λ.

2.2 Semi-Empirical Formulation of Absorption and Scattering Equations

Shamanaeva's approach to modeling the total attenuation coefficient is similar to that presented in equation (2), where the total attenuation coefficient can be divided into its molecular and turbulent scattering elements.

The classical component of the acoustic absorption coefficient (α_{cl}, in units of m^{-1}) represents the combined impact of viscosity, heat conduction, diffusion, and energy transfer from the acoustic wave to molecular rotational modes. It is given by the empirical relation

$$\alpha_{cl} = 4.02 \times 10^{-11} f^2 \cdot \tag{6}$$

In addition to the classical absorption coefficient, there is an even larger (at ultrasonic frequencies) molecular absorption coefficient (also in units of m^{-1}). To formulate this term, one first evaluates the frequency of maximum molecular absorption due to energy transferring from acoustic waves to the lowest excited vibrational molecular states of diatomic oxygen and nitrogen. This frequency maximum is given by the semi-empirical expression

$$f_{Max}(z_i) = \left[10 + 6600\, h_0(z_i) + 44400\, h_0^2(z_i)\right] P_1(z_i) / T_1^{0.8}(z_i)\,, \tag{7}$$

where

$$\begin{aligned} P_1(z_i) &= P(z_i)/1014\,, \\ T_1(z_i) &= (1.8\,T(z_i) + 492)/519\,, \\ h_0(z_i) &= 100\, e_1(z_i)/P(z_i)\,, \\ e_1(z_i) &= 0.06107 \times 10^{M_1(z_i)} U(z_i)\,, \\ M_1(z_i) &= 7.63\,T(z_i)/[241.9 + T(z_i)]\,. \end{aligned} \tag{8}$$

Here, z_i represents the height at which the calculation is performed, since most atmospheric properties vary primarily with height above the surface. In the analysis to follow height is set at 1-m above ground level (AGL) for consistency with our early measurements. Other meteorological parameters are the relative humidity, $U(z_i)$, in percent; atmospheric pressure, *P*,

in millibars (mB); temperature, *T*, in degrees Centigrade (°C). The ubiquitous appearance of the *i* subscript allows for a layered atmosphere within the computer model.

The first term in equation (7) represents the relaxation frequency for oxygen and nitrogen collisional absorption in dry air. The second term is associated with oxygen/nitrogen collisional interactions with water vapor and the third term addresses the effects of collisional interactions between water vapor molecules.

At the peak frequency, f_{Max}, the maximum molecular absorption coefficient is given by

$$\alpha_{Max}(z_i) = 0.0018\ f_{Max}(z_i)\, T_1^{-2.5}(z_i) \exp\left\{7.77[1 - T_1^{-1}(z_i)]\right\}. \tag{9}$$

These two parameters can then be used in modeling the general molecular absorption coefficient (expressed in m^{-1} units) as,

$$\alpha_{mol}(z_i) = \frac{\alpha_{Max}(z_i)}{304.8}\left(\left[0.18\, f_k(z_i)\right]^2 + \left[\frac{2\, f_k^2(z_i)}{1 + f_k^2(z_i)}\right]^2 \right)^{1/2}, \tag{10}$$

where another dimensionless parameter is introduced:

$$f_k(z_i) = f\ /\ f_{Max}(z_i)\,. \tag{11}$$

The total absorption coefficient is obtained by summing equations (6) and (10), i.e., $\alpha_a = \alpha_{cl} + \alpha_{mol}$.

For turbulent scattering effects, Shamanaeva (2004) used the von Karman turbulence spectrum to evaluate volume scattering functions for temperature and wind coefficients, $\alpha_t = \alpha_T + \alpha_V$, given in the form,

$$\alpha_T(z_i) = 0.9\, \lambda^{-1/3}(z_i)\, C_T^2(z_i)\, T^{-2}(z_i)\, L_0^{-7/3}(z_i) \left\{ \begin{array}{l} 0.07143\left[B^{7/6}(z_i) - \lambda^{7/3}(z_i)\right] \\ \quad -0.1A^2(z_i)\left[B^{-5/6}(z_i) - \lambda^{-5/3}(z_i)\right] \\ \quad -A(z_i)\left[B^{1/6}(z_i) - \lambda^{1/3}(z_i)\right] \end{array} \right\}, \tag{12}$$

$$\alpha_V(z_i) = 1.569\, \varepsilon^{2/3}(z_i)\, \lambda^{-1/3}(z_i)\, c^{-2}(z_i)\, L_0^{-13/3}(z_i) \quad \times$$

$$\left\{ \begin{array}{l} 0.1429\left[B(z_i) + 2A(z_i)\right]\left[B^{7/6}(z_i) - \lambda^{7/3}(z_i)\right] \\ \quad -0.0769\left[B^{13/6}(z_i) - \lambda^{13/3}(z_i)\right] \\ \quad -A(z_i)\left[A(z_i) + 2B(z_i)\right]\left[B^{1/6}(z_i) - \lambda^{1/3}(z_i)\right] \\ \quad -0.2A^2(z_i)\, B(z_i)\left[B^{-5/6}(z_i) - \lambda^{-5/3}(z_i)\right] \end{array} \right\}, \tag{13}$$

introducing parameters,

$$A(z_i) = 2L_0^2(z_i) + \lambda^2(z_i)$$
$$B(z_i) = 4L_0^2(z_i) + \lambda^2(z_i) \quad . \tag{14}$$

Here, $\lambda(z_i)$ is the acoustic wavelength at height z_i , $c(z_i)$ is the speed of sound, $L_0(z_i)$ is the outer scale of turbulence, $C_T^2(z_i)$ is the structure parameter of the turbulent temperature field, and $\varepsilon(z_i)$ is the dissipation rate for turbulent kinetic energy. The temperature structure parameter may in turn be derived from the more familiar refractive index structure parameter $C_n^2(z_i)$ via the expression,

$$C_T^2(z_i) = C_n^2(z_i)\left(\frac{(T+273.15)^2}{7.95\times10^{-5}P}\right)^2 . \tag{15}$$

As an initial study, meteorological parameters were set to values consistent with our earliest outdoor WSMR-measurements of acoustic extinction conducted on the afternoon of 6 Nov 2008. The ambient conditions present were: relative humidity, $U(z_i)$ = 12%; pressure, P = 880 mB; temperature, T = 13.3 °C (56 °F). The WSMR-area value for the refractive index structure constant was estimated for the appropriate time of day (approximately 1600) using a model derived from the High Energy Laser Propagation Handbook (Hummel, 1984); this value was estimated as $C_n^2(z_i) = 8.1\text{x}10^{-15}$ m$^{-2/3}$. The outer scale was set equal to the height of the transmitter/receiver setup: z_i = 1 m. A nominal daytime dissipation rate of $\varepsilon(z_i) = 5\text{x}10^{-3}$ m^2 s^{-3} was selected based on Stull (1988) for use in computing the wind scattering coefficient of equation (13).

However, relative humidity data were not taken directly. Instead, humidity data were obtained from a nearby surface station. The sensitivity of equations (7) through (11) to humidity variations is highlighted by figure 1, which displays the total absorption coefficient as a function of relative humidity at an acoustic frequency of 20 kHz for the temperature and pressure conditions indicated. The total absorption curve is the sum of the classical (equation 6) and molecular (equation 10) results. For all but the lowest relative humidities, the molecular absorption effect is dominant. The nominal relative humidity of 12% for our example case yields a total absorption coefficient of 0.054 m^{-1} (or about 0.24 dB m^{-1}). Note from equation (7) that the relaxation frequency f_{Max} is essentially constant at very low relative humidities and increases very rapidly at high relative humidities. Thus, for the fixed ultrasonic acoustic frequency f, the molecular absorption coefficient versus relative humidity curve will show a peak for those relative humidities where the relaxation frequency f_{Max} approaches f. This peaked behavior is also seen at some the higher acoustic frequencies displayed in table 1.

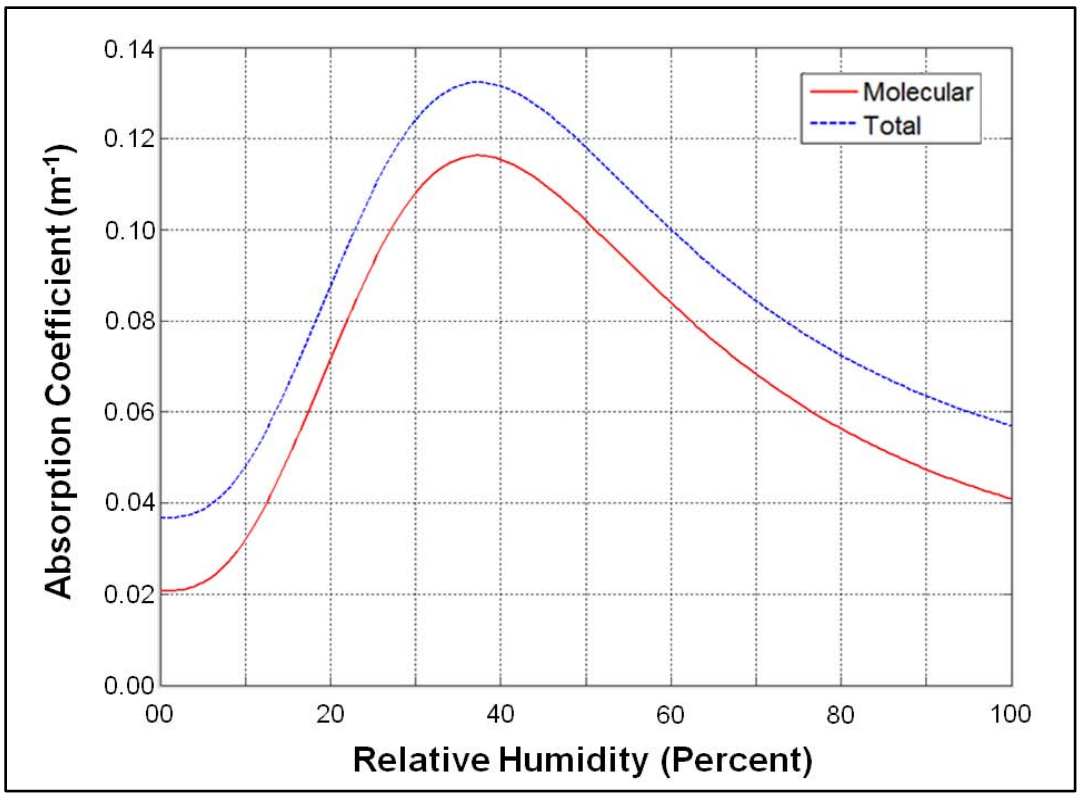

Figure 1. Absorption coefficient versus relative humidity at f = 20 kHz (P = 880 mB, T = 13.3 °C).

The scattering coefficients for wind and temperature turbulence given by equations (12) through (15) are compared with the total absorption coefficient as a function of acoustic frequency in figure 2.

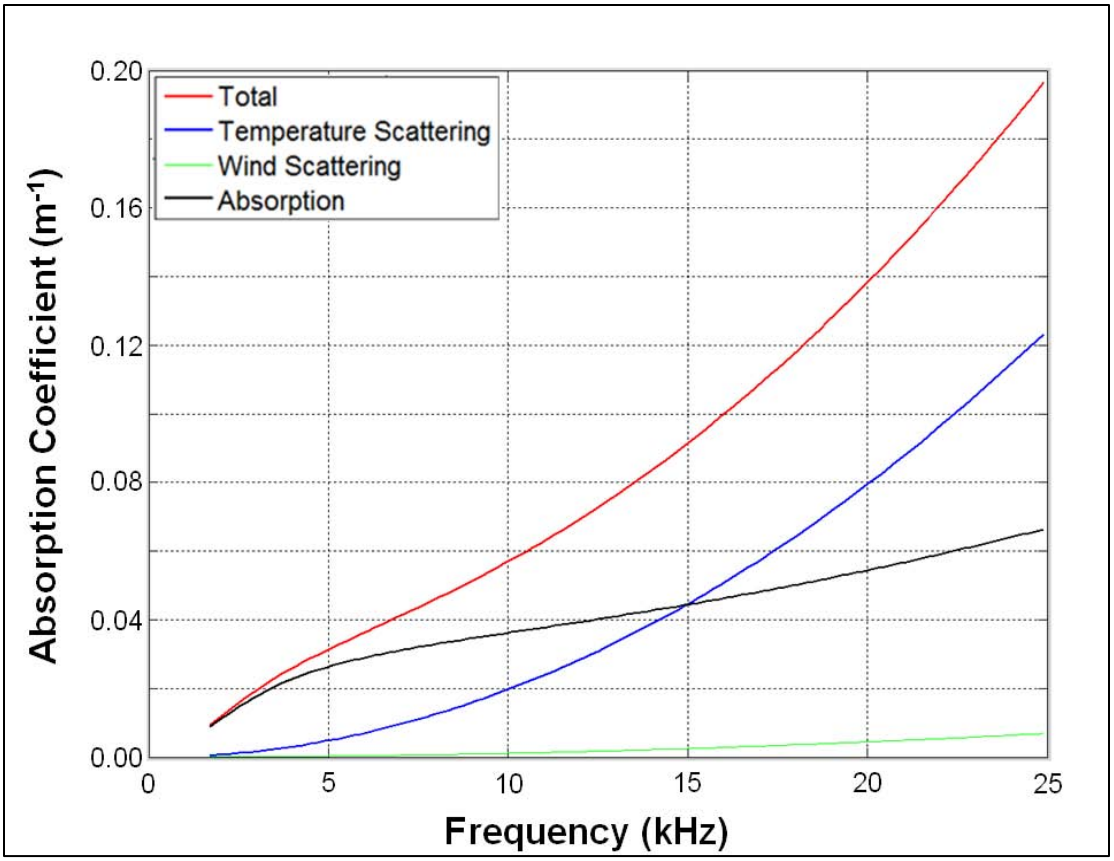

Figure 2. Total, temperature scattering, wind scattering, and total absorption coefficients as a function of frequency for the example case.

As noted by Baikalova et al. (1988), both the temperature and wind turbulence scattering coefficients exhibit a quadratic increase with frequency, a trend that is evident in figure 2. This behavior is readily seen in equations (12) and (13) by noting that for most practical observation heights z_i, $L_0 >> \lambda$ at ultrasonic frequencies, since L_0 is on the order of meters, while λ is on the order of centimeters or less. Thus parameters A and B (equation 14) are practically constant with frequency, and the dominant terms in the quantities in brackets in equations (12) and (13) are those containing the $\lambda^{-5/3}$ factor. Baikalova et al., also note that these scattering coefficients scale as $L_0^{5/3}$, again due to the dominant terms containing the $\lambda^{-5/3}$ factors in equations (12) and (13).

2.2 Comparisons of Attenuation Data with Models

Our initial outdoor experiments were conducted using a very simple ultrasonic transmitter and a bare microphone SPL meter receiver. The SPL instrument's output used a simple analog needle panel meter that had to be manually read and recorded. Figure 3 compares the observed SPL data with inverse square curves chosen to intersect with the 1-m range data.

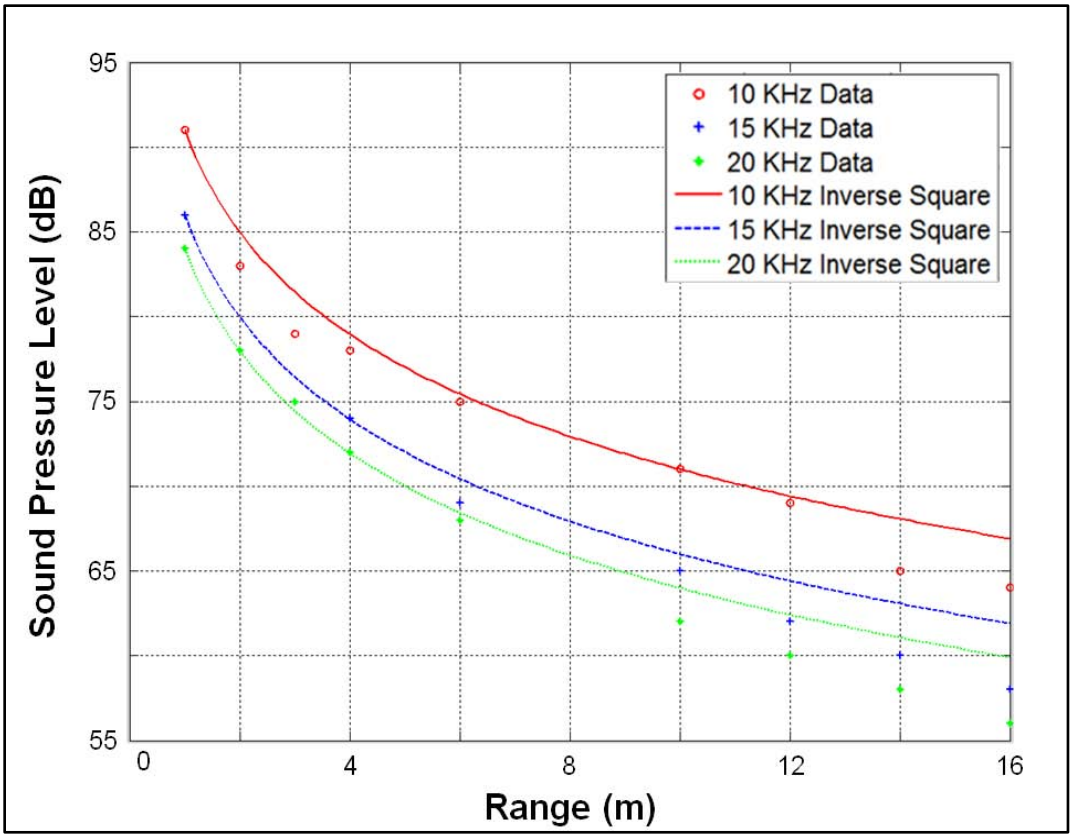

Figure 3. Comparison of SPL measurements with inverse square curves at 10-, 15-, and 20-kHz acoustic frequencies, 06 Nov 2008.

Figure 4 shows least squares power law fits to these data. The inverse square trend was removed from the data in figure 5. Note the increased scatter in these detrended results, which is possibly indicative of reflected energy contributions.

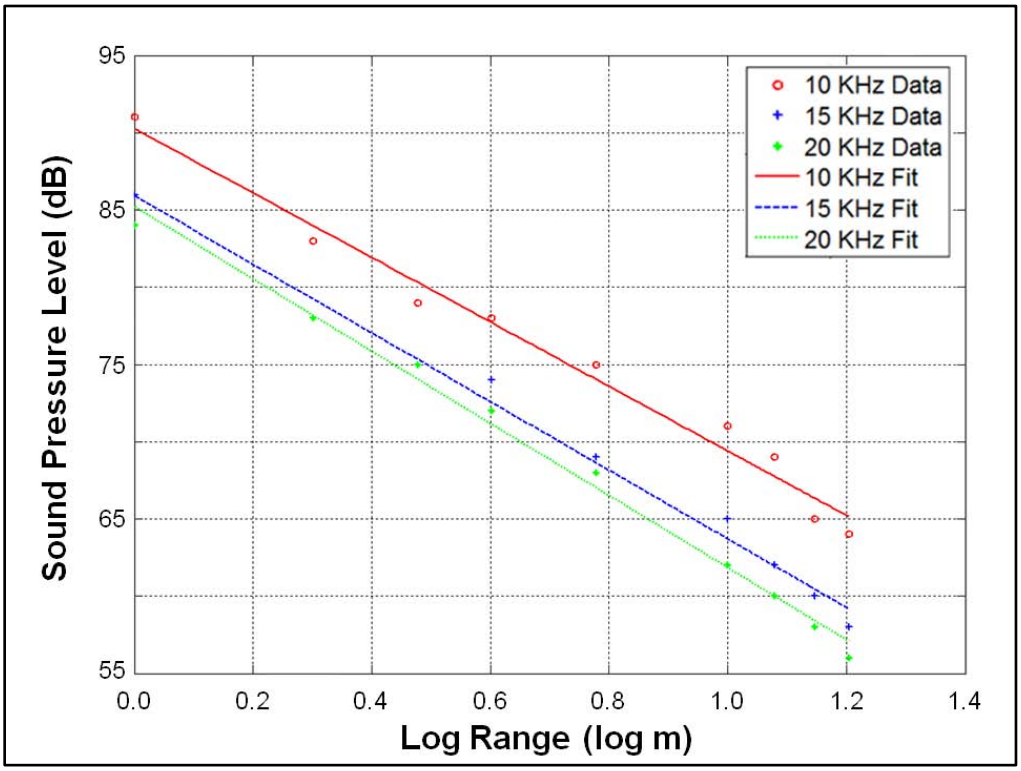

Figure 4. Power law fit to measured SPL data, 10-, 15-, and 20-kHz acoustic frequencies, 06 Nov 08.

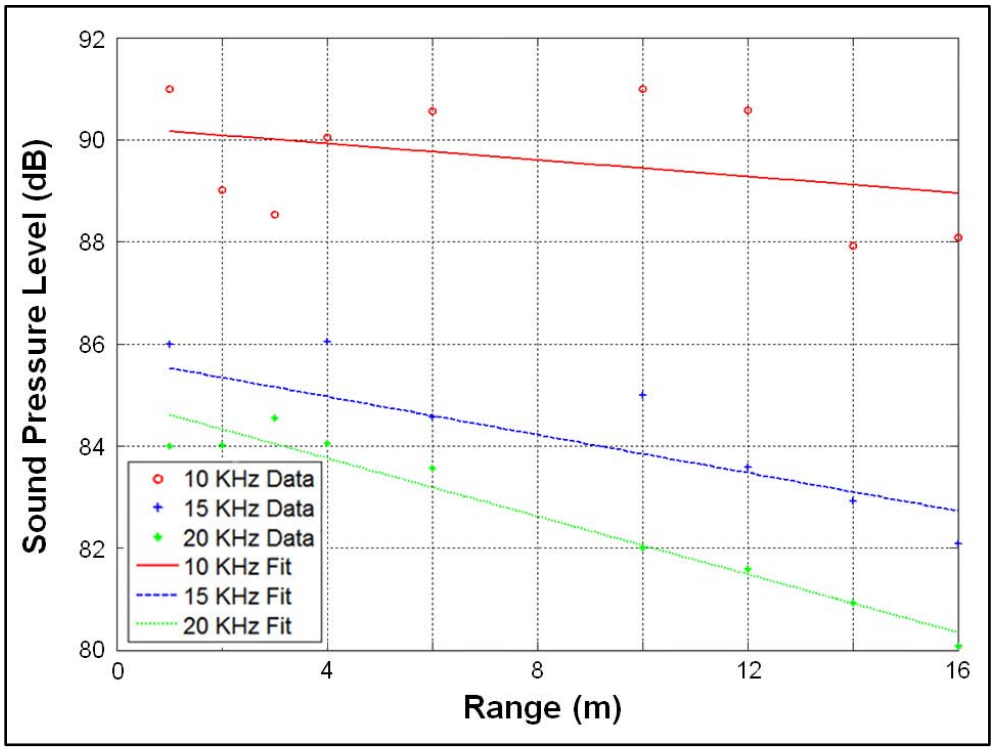

Figure 5. SPL field measurements with inverse square trend removed and fitted with a power law curve, 10, 15, and 20 kHz, 06 Nov 08.

The SPL data plots indicate that most of the attenuation observed was due to inverse square spreading from the quasi-point source. The residual plot of figure 5 provided values for attenuation coefficients at the measured frequencies in table 2.

Table 2. Residual attenuation coefficients computed from data of figure 5.

Frequency (kHz)	Attenuation (dB/m)	Attenuation (m^{-1})
10	0.08	0.018
15	0.19	0.044
20	0.28	0.064

Comparing the results of table 2 with the model predictions of figure 2, it is apparent that the observed attenuation coefficients are considerably smaller than the modeled total attenuation. However, these early observations did not have any direct measurement of turbulence from which C_T^2 could be estimated. There is also the strong possibility that ground surface reflections could have significantly contributed to the received SPL signal. It is true that the observed residual values of table 2 are comparable to the individual total absorption or wind turbulence scattered signals.

Another factor affecting scattering behavior in this spectral range is the nominal ultrasonic probe wavelength. For a typical speed of sound of c_0 ~340m/s, a 20-kHz probe frequency yields a propagation wavelength on the order of ~1.5 cm. This equates to a wavenumber $\kappa_s = 2k = 4\pi/\lambda = 831\,\mathrm{m}^{-1}$. These probe wavelength and wavenumber values are on the order of those that are characteristic of the inner scale of boundary layer turbulence, which has wind-dependent values that range from roughly 2–8 mm for length ℓ_o or 125–500 m^{-1} for the $\kappa_s \approx 1/\ell_o$ wavenumber. We might thus be able to avoid some deleterious path related scattering by increasing the probe frequency. This will, however, have little effect on Doppler shifting of signals due to along-path wind speed variations and will not be able to avoid increased attenuation (see table 1) due to molecular absorption effects.

Microphone noise due to atmospheric density fluctuations advecting past a sonic receiver was also studied as a potential problem during our measurements. After some consideration, it was decided that such noise would not present a significant obstacle. Since ambient density fluctuations will have size scales comparable to the inner scale (a few millimeters) or greater, and average wind speeds will be typically less than 8 m/s (less than 15 mph), it is expected that the bandwidth of acoustic fluctuations should be on the order of 8 kHz (8m/s/1mm = 8 kHz). Testing at short range or with no external signal source present did not produce noticeable noise signals at frequencies over 10 kHz (though typically measurements have been taken on calm days so far). Unless high frequency noise sources are located within a short range of the receiver, it is also expected that strong atmospheric attenuation will suppress such noise

signatures. Hence, we do not expect to encounter strong atmospheric high frequency noise sources within range of a receiver.

We may summarize our assessment of atmospheric effects upon ultrasonic propagation as the following: For propagation paths out to 30 m the losses incurred in the signals due to radial velocity, molecular, and scattering effects do not appear to significantly impede useful signal transmission. Even 30-dB losses are well within the limits for many typical acoustic detection systems to handle. Of more critical interest is the actual dynamics of testing an acoustic communications system as described next.

3. Infrastructure Development

As discussed in section 1, a program was developed to consider feasibility of ultrasonic communications in a field environment. The set of experiments that evolved from this concept took place primarily during the late fall of 2009, a time of year that was fortuitous for milder weather conditions that generally prevail throughout the October through November period in southern New Mexico.

3.1 General Site Description

The site chosen for the setup of the main testing of the prototype communications system developed was the building 19472 compound (figure 6) to the south of the main cantonment area of WSMR. The region surrounding this compound is relatively flat and treeless terrain characteristic of the high Chihuahuan desert. The main vegetation found are the yucca and creosote bushes, both standing approximately a meter high, interspersed with wide grasses and redroot pigweed (*amaranthus retroflexa*). The dirt is alluvial, derived from sand eroded from the nearby Organ Mountains. The proximity of the mountains creates a slight tilt in the general terrain due to the alluvial skirt, affecting the local vertical for wind flow considerations. The GPS location for building 19472 is: N 32° 21’ 15.4’’, W 106° 27’ 57.7’’.

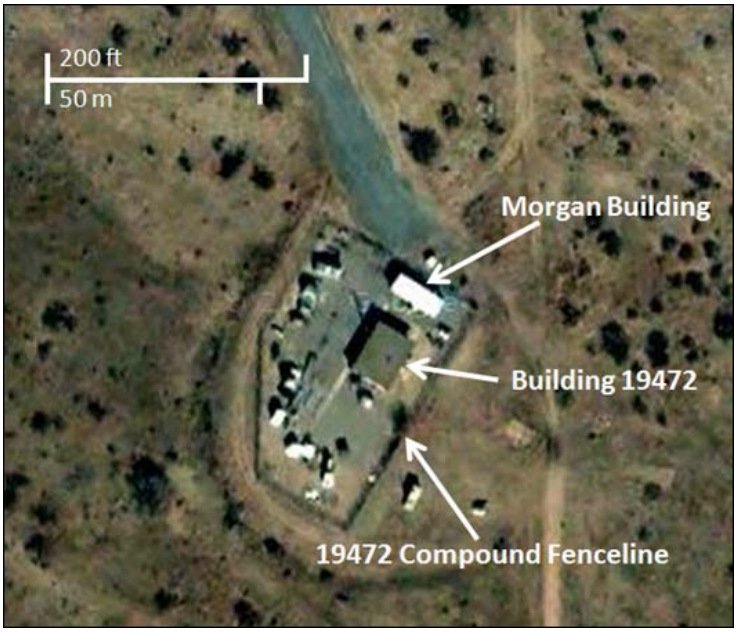

Figure 6. Building 19472 compound on WSMR, NM, and its environs.

Although the site is nearly flat, there are a few nearby perturbing features to optimal smooth-terrain wind flow. These are located primarily to the east-southeast and the southwest of the compound involving a minor gully (arroyo). The 19472 compound itself, as shown in figure 6, consists of the single story main building surrounded by a number of parked trailers, small storage shelters, vehicles, a Morgan storage building, and a chain-link fence enclosure. For scale perspective, building 19472 measures 44 ft×32 ft (the building's shadow is visible within the compound), the southeast fence line measures 201 ft, and the NNE fence line measures 136 ft, and the southwest corner of building 19472 is 73 ft from the WNW corner of the fence line.

In the figure 6 satellite image, the dark dots seen scattered about the outside of the fence line are relatively intermittent but significantly-sized mesquite bush patches that are approximately 2 m high and up to several meters wide. A thicket of these bushes is contained within a shallow arroyo to the west and south of the site.

A series of improvements were made to the 19472 site for the ultrasonic communications tests. Among these was a general clean up of equipment left over from previous projects and the installation of a scaffold near the main gate of the compound (figure 7). This scaffold permits the taking of acoustic data from a height of approximately 4-m AGL. By placing the receiver at this height, the influence of ground reflections (multipathing) can be minimized. Removing this effect from the received signals was believed to be a significant step in decoupling the impacts of molecular attenuation, multipathing, and atmospheric turbulent scattering from the resulting propagated signal strengths in testing.

Figure 7. Acoustic path receiver scaffold used in power vs. range testing at 19472 site. The top of building 19472 is seen in the background. Acoustic receiver is seen at the top of the scaffold's second level.

Additionally, the road leading to the 19472 site was recently paved, allowing us to apply permanent painted markers to the roadway so that specific propagation slant paths can be repeated based on distances measured to a receiver mounted on the scaffold's upper level. The site therefore provides repeatable conditions for future prototype testing.

Unfortunately, while these site preparations were underway, a serious electrical safety accident occurred at an ARL testing facility at Aberdeen Proving Ground that significantly impacted our test planning. As a result of that fatal accident, ARL field testing operations were suspended until the safety procedures for all testing facilities within ARL could be reviewed and recertified and all personnel retrained in electrical safety. In response to this review, a series of precautions and training actions were taken as indicated in the following section.

3.2 Safety Concerns, Preparations, and Training

In order for any field experimentation to be successfully completed, an evaluation of the risks involved must be conducted prior to implementation of the study. As the test plan is being drafted, and the risk analysis has been performed and reviewed, the personnel involved must be briefed on the safety concerns. Before undertaking the test, it must be confirmed that all involved personnel have current safety training tailored for the particular tasks of the field test.

For this test, areas of concern were scaffolding use, electrical safety, and ultrasonic effects on human hearing at the frequencies and power levels of interest. To ensure that the best possible working environment was in place, ARL safety was involved in the risk analysis and in

reviewing the safety standard operating procedure (SOP) developed for the test (see the appendix).

To address the scaffolding safety issue, all personnel involved were required to complete the OSHA training regarding scaffolding prior to operations with the tower at building 19472. The tower had already been emplaced some time before the attendant heightened safety concerns had been raised, so during the subsequent safety stand-down period and before the final ARL approval of the new safety SOP, no use of the scaffold was made.

The electrical safety issues were addressed by having the involved personnel take a series of several ARL electrical safety training sequences including laboratory and field operations and evaluating the electrical risk for the test. The electrical risk for this test was low, as the power levels involved are relatively small. Also, the systems in use are all UL approved commercial off-the-shelf (COTS) components.

The effect of ultrasonic radiation on human hearing was also researched and the results of those findings were included in the safety SOP for review and approval. As analyzed, such effects would only be significant if the sound was being propagated under water or at sound intensity levels approximately one hundred times more powerful than those used in these tests. Therefore, the energy levels for this testing were sufficiently low that the safety concerns were minimal. This is also a valid operational conclusion as well. It is not expected that the use of such devices would be harmful to troops under operational circumstances.

The required safety controls for site access during testing, however, did affect physical security at the site. To ensure that only authorized or permitted personnel are on site during testing, a checks system was initiated to ensure that the system was not energized while personnel were in locations that would subject them to the highest levels of energy.

Summarizing, all test personnel completed the mandatory training for this type of work, which included OSHA scaffolding use and/or installation training as well as ARL's electrical safety for field experimentation sequence.

3.3 Angular Antenna Pattern Testing

As a preliminary development, a set of acoustic horns representing different form factor designs was purchased to assess the impact of form factor upon ultrasonic emission patterns in different acoustic propagation regimes. For instance, when focused energy needs to be propagated, a narrow horn would provide a better concentration of acoustic energy than a wide horn. On the other hand, when propagating a signal for detection purposes when wind effects might tend to deflect a tight beam off a point receiver, a narrow horn might not be the best option. In this case, a wider pattern source beam is desirable.

To characterize this series of horns (plus an emitter mounted to a parabolic dish), a series of measurements were performed on each. This testing was conducted on an angular layout

positioned between building 19472 and the “Morgan” storage building of the 19472 compound. The distance from the emitter to the microphone was 8 ft 8 inches, and the microphones were then moved off axis in +/–15 degree steps all the way to 90 degree off axis point. The complete scan went from 0 degrees, to +90 and –90 degrees off axis for each antenna tested. The main detection instrument used for these measurements was the SPL meter. A continuous tone was broadcast for 30 seconds for each angular setting. The mean SPL value was then post-processed using a spreadsheet program in Linux. For these experiments an additional uncalibrated microphone with very flat response and good ultrasonic sensitivity was also used for future comparison purposes as seen in figure 8.

Figure 8. SPL sensor microphone (bottom) and uncalibrated microphone configuration.

A photograph of each horn (along with the parabolic dish) and its measured antenna pattern are depicted in figures 9–16.

Figure 9. “Trumpet”-style horn (narrow beam).

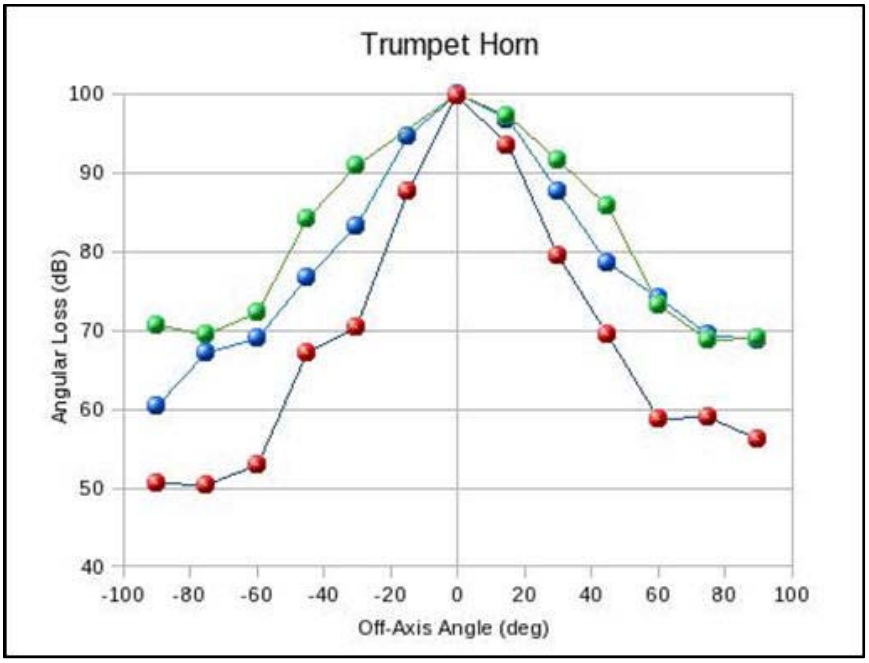

Figure 10. "Trumpet" horn antenna pattern. Sonic intensities at 5-, 10-, and 20-kHz frequencies (green, blue, and red lines, respectively).

Figure 11. Parabolic dish (narrow beam).

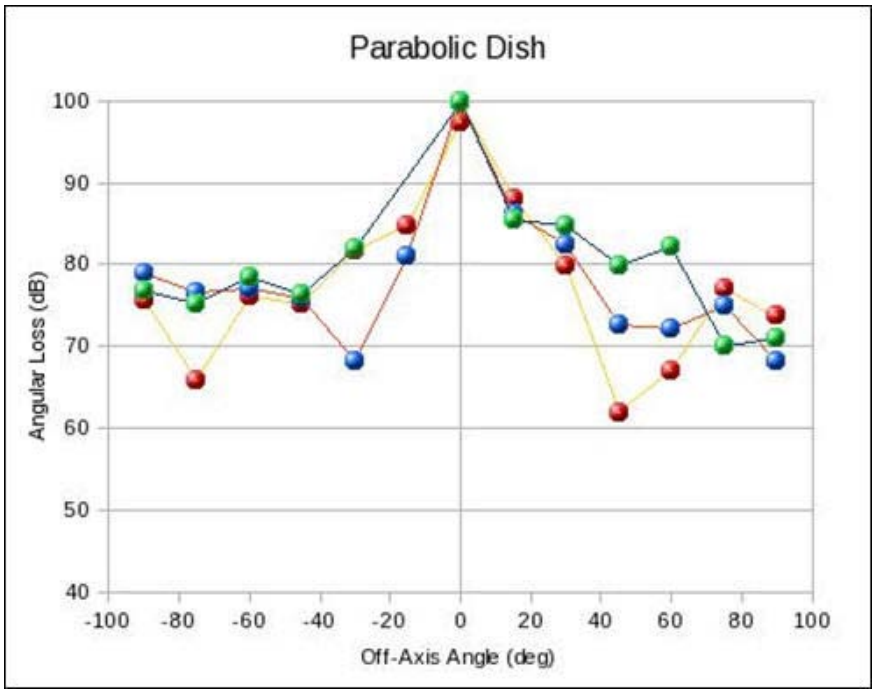

Figure 12. Parabolic dish antenna pattern. Sonic intensities at 5-, 10-, and 20-kHz frequencies (green, blue, and red lines, respectively).

We note that the antenna patterns of the trumpet horn and the parabolic dish provide the two narrowest patterns at small angle. However, while the parabolic dish supplies a very rapid drop at small angles, it does not continue to drop. Rather, it plateaus at approximately a –25 dB loss, while the trumpet horn pattern, particularly at the highest frequency range (20 kHz) exhibits a very high attenuation at large off-axis angles approaching –50 dB.

Figure 13. Round (wide mouth) horn.

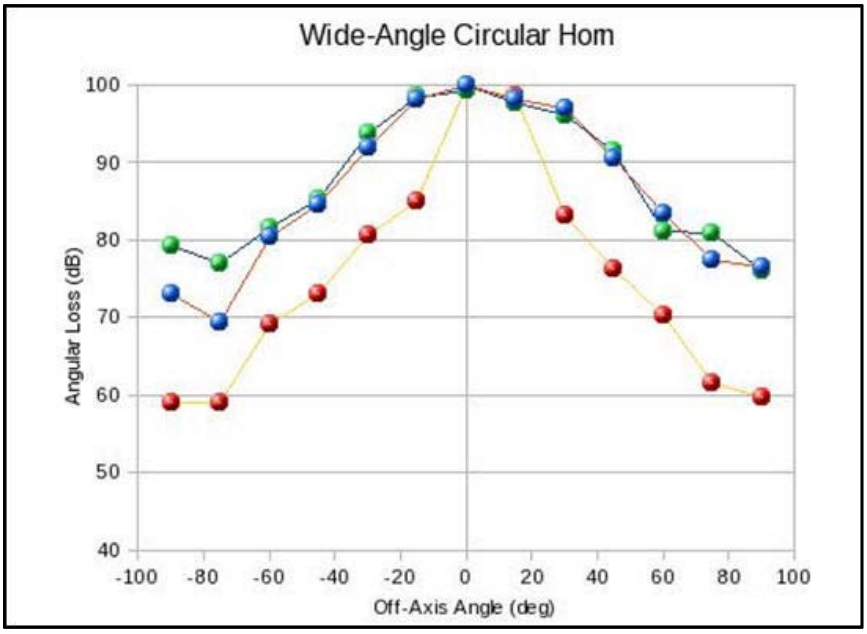

Figure 14. Round horn antenna pattern. Sonic intensities at 5-, 10-, and 20-kHz frequencies (green, blue, and red lines, respectively).

Figure 15. Rectangular (wide mouth) horn.

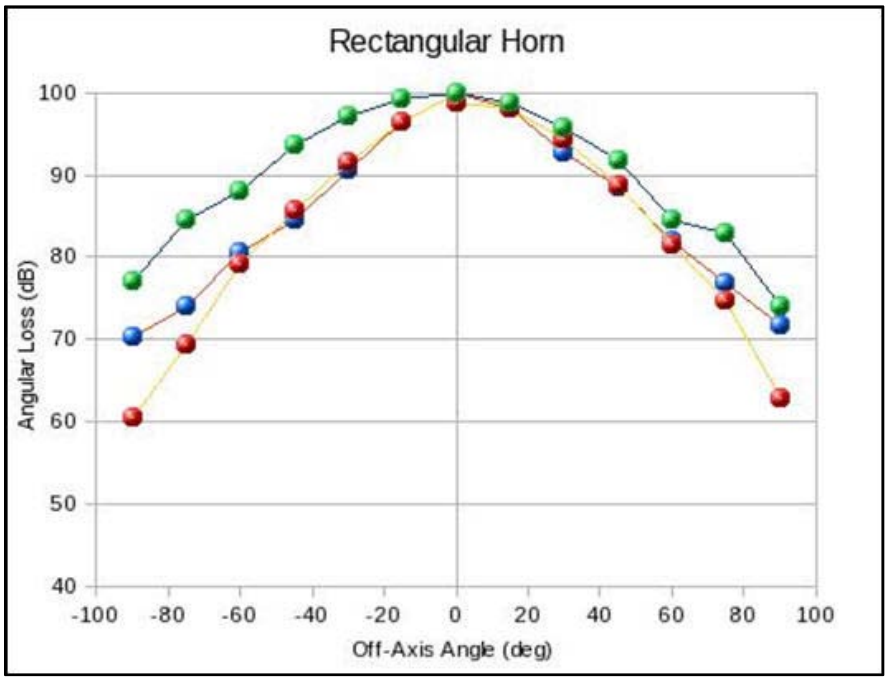

Figure 16. Rectangular horn antenna pattern. Sonic intensities at 5-, 10-, and 20-kHz frequencies (green, blue, and red lines, respectively).

We note that the pattern specified for the rectangular horn was measured in the plane that contained the widest aperture dimension. This plane is tilted slightly from horizontal in figure 15.

In comparing the patterns of the two wide-angle horns, it is interesting to note the differences. While the rectangular horn appears to exhibit similar behavior for both the 10- and 20-kHz results, the 20-kHz case for the round horn is significantly more focused than the results of either 5- or 10-kHz signals. Based on this behavior, the rectangular horn appears to be more frequency independent, which should be more useful in testing cases involving broadcast signals that we intend to disperse uniformly in angle.

4. LabVIEW Software Developments

In order to conduct the necessary experiments for our research, a variety of tools were assembled to characterize and implement the communication system process. These include hardware for transmission, reception and measurement of acoustic signals, meteorological sensors to measure atmospheric conditions, as well as software codes to generate signals, support the data acquisition of these signals, and analysis codes to assess the quality of transmission channels under varying meteorological conditions. These functions were integrated into laptop computer systems that hosted software control of hardware, data acquisition, and data analysis.

The signal generation and data collection for propagation studies were accomplished using control software based on the National Instruments (NI) LabVIEW program. LabVIEW is a general instrument control program that utilizes a visual programming language suitable for receiving, filtering, and manipulating data streams in user-configured applications termed "virtual instruments" (VI). Each VI simulates a system through a graphically correct "Front Panel" that includes computer simulated control devices (slider bars, control knobs, switches, etc.) that implement the functionality of the measurement and control interface. This Front Panel is then connected to a virtual circuit board (termed the "Block Diagram") that emulates the functional interconnections behind an actual instrument panel. LabVIEW provides a series of user designated processing elements on the block diagram that effectively simulate the logic and control operations of a traditional programming language. The principal difference between LabVIEW and an abstract language is that LabVIEW connects to real instrumentation through NI hardware interface modules that are controlled by the LabVIEW software.

Two VIs were developed for testing purposes. One VI functioned as a waveform generator to create tones of a specified frequency, amplitude and duration. This tone formed the test signal, and was sent through an analog output to an emitter amplifier and then to a speaker with attached focusing horn. A second VI acquired and logged the measured data from a SPL meter. Data from a sonic anemometer was also logged by this VI for future analysis, allowing the sound data

to be correlated to variations in wind speed, direction and/or turbulence. Measurements from both the SPL meter and sonic anemometer were synchronized and time stamped, then saved to disk at a sample rate of 20 Hz.

The front panel of the emitter controller is shown in figure 17. The figure illustrates the control widgets that select the signal duration, frequency, amplitude, and sampling rate. In figure 18 the front panel of the SPL data collector is shown. The upper portion of the front panel controls the input data ingest from the SPL meter, while the lower portion monitors the port interface, windowed data, and storage for the sonic anemometer data. The "base spl" control indicates the minimum reading level allowed by the meter (set through a hardware control knob on the meter itself) plus a file name in which the data is stored. L2W sets and indicates the sampling rate for data collection. In the lower portion of the SPL collector VI panel, the critical elements are the data baud rate produced by the sonic anemometer sensor output interface and the input port address.

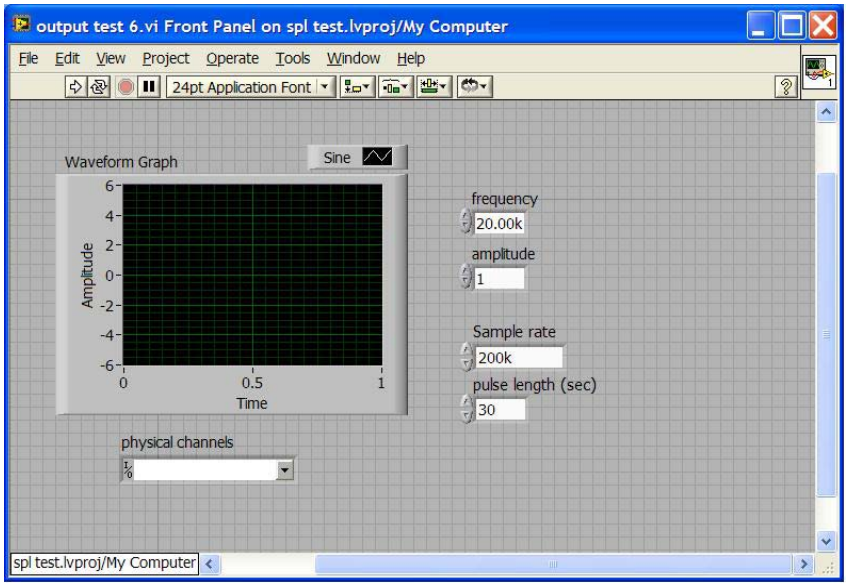

Figure 17. Front panel for signal generator used in dispersion experiments.

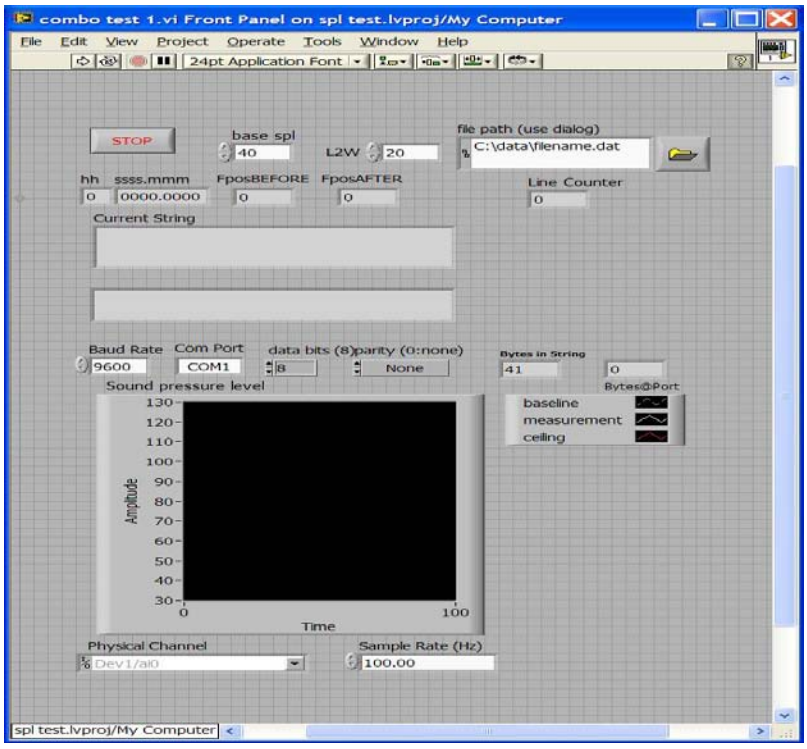

Figure 18. Front panel for SPL and wind measurements used in dispersion experiments.

The ultrasonic emitter hardware consisted of a Motorola Powerline piezoelectric horn driver mounted to an appropriate horn (usually the rectangular aperture horn since it has the widest dispersion pattern and lowest frequency sensitivity). The driver/horn system was fed by a small computer speaker amplifier in this series of tests. The amplifier/driver system can produce acoustic energy at frequencies from 1.8 to 30 kHz, and was effective for most of the signal generation needs of our program. The sound pressure levels were measured by a Quest model 155 sound level meter equipped with an OB-133 1/3 octave filter. Both the signal output to the amplifier and the input from the sound level meter were routed through an NI USB-6281 multifunction data acquisition (DAQ) module. This data acquisition system allows multichannel collection of up to 500-k samples per second at 18-bits accuracy, with transmission of up to 1-M samples per second at 16-bits accuracy, and can fulfill data acquisition needs for many applications. The sonic anemometer used was an R. M. Young model 81000 device. RS-232 formatted data transmitted by this device was also recorded from the COM1 serial port of the computer.

After the preliminary measurements that characterized the sound intensity patterns emerging from the three horn devices and the parabolic reflecting dish were made, propagation measurements were then performed using LabVIEW transmitter/receiver control and analysis codes that we developed. These codes characterized the general influences of range attenuation

due to $1/r^2$ losses, atmospheric absorption of sonic energy, and acoustic scattering of sound as a function of range. These results are described in section 2.

A subsequent LabVIEW code development phase involved the building of a rudimentary communications system to allow the functional testing of the feasibility of ultrasonic modulation of digital signals. Here, a LabVIEW VI was designed to modulate and demodulate ultrasonic waveforms such that ASCII character data would be transmitted. This software was initially developed using AM pulsing, but was then adapted to perform FSK modulation.

The transmitting software decomposed a string of ASCII characters into equivalent byte strings and added start and stop framing bits to the end of each byte, as in the RS-232 protocol. The software then encoded each bit as a pulse of ultrasonic sound at the appropriate frequency. In the AM mode, only "1" bits would be transmitted at the carrier frequency. In the FSK implementation, the "0" and "1" bits were each assigned unique carrier frequencies.

The hardware used for data transmission in this study was the same as used for signal emission during the emission pattern propagation tests. However, on the receiver side of the data transmission tests, the SPL meter was replaced by a high fidelity Earthworks M50 measurement microphone, used in conjunction with a Grace Design M101 preamplifier. The M50 microphone was particularly suited to our measurement program due to its very flat frequency response between 5 Hz and 50 kHz, amounting to a ripple of less than 3 dB over this frequency range. The preamplifier used in this phase of our investigation allowed a very wide range of measurement with 65 dB adjustability in signal gain. The signal from the preamplifier could be acquired either by the USB-6281 used by the transmitter, or an NI Compact DAQ modular chassis with an NI 9205 module. The Compact DAQ chassis is more affordable, but is limited to 250-kilo samples per second with 16-bit accuracy for input measurements using the NI 9205 module.

The receiving software VI module was then designed to listen continuously on a microphone input for a signal on the "1" carrier frequency, used by the start bit of each byte. Upon identification of a clear tone of this frequency, the receiver software was then programmed to collect a 10-bit signal string appropriate for one ASCII byte. At the end of each bit, the data received is analyzed for frequency and assigned a 1 or 0 value depending on an assessment of which frequency it most strongly matched. Upon collecting all 10 bits, the bits were reassembled into an ASCII byte value and output to a string updated continuously in the "String" box of the software front panel as shown in figure 19.

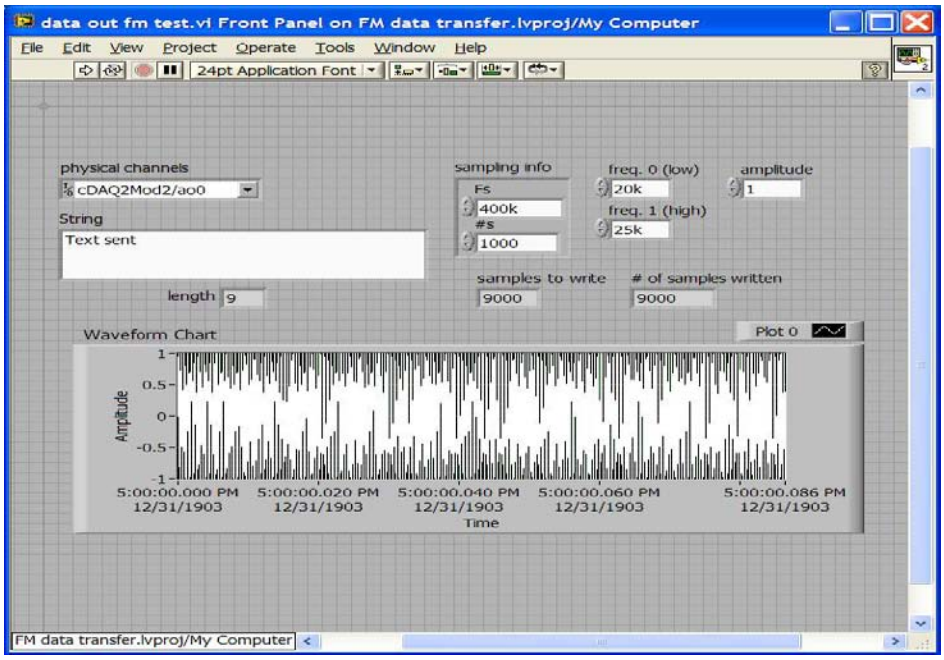

Figure 19. Front panel for FSK data transmitter.

Figure 19 also indicates that the user can dynamically select the identities of the frequencies used for encoding the 0 and 1 bits. As an example of the wiring diagram methodology used to implement the LabVIEW block diagram construct, we depict the structure of the FSK transmitter code in figure 20. The main features of interest in this code diagram are the large outline boxes on the right side of the figure. These represent a double looping structure associated with the process of decomposing each ASCII character (outer box) into its individual bits and encoding these (inner box) onto a general data stream that is then output to the string of small boxes to the right of the main boxes.

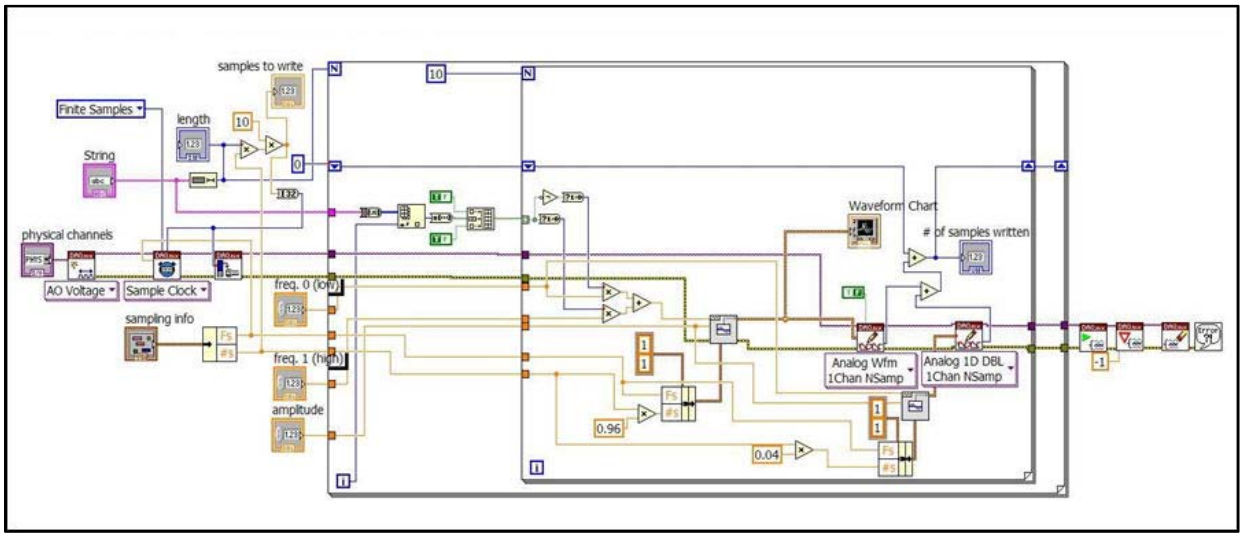

Figure 20. Block diagram of FSK data transmitter.

These smaller boxes represent the transfer of the main data buffer to the NI DAQ hardware. The boxes at the left of the main boxes represent control and data buffer initiation steps needed to generate the data buffer and determine the nature of the subsequent encoding of the data bits.

To determine the fidelity of the data transmission process a series of tests were performed using the above equipment. The results of these tests are described in the following section.

5. Propagation and Communications Characterization

Following the development of safety standards and prototype software models of transmitted power and communication systems, the tools described in the previous section were tested at the building 19472 site to determine the feasibility of an ultrasonic communication system. The first stage of this testing was a rather simple task, designed to benchmark the capabilities of the system to detect single-frequency sound levels as a function of range. The primary objective was to determine the validity of a model predicting molecular absorption rates of ultrasonic signals. To test this model we performed a series of tests along the road leading into the 19472 compound.

5.1 Slant-Path Propagation Tests

The purpose of these measurements was to achieve a more comprehensive and workable understanding of the general loss of signal with range at different frequencies across the audible and ultrasonic ranges (up to 24-kHz frequency). The primary loss mechanism would be the $1/r^2$ loss rate associated with the near-spherical wave expansion of the initial beam. The secondary loss mechanism was originally believed to be the molecular attenuation effect. However, it became apparent that turbulent scattering losses are also significant, even at short range.

The power transmitted was measured for a set path at different frequencies (4, 8, 12, 15, 16, 20, 23, and 24 kHz). Readings were collected using the SPL meter and logged by the LabVIEW software controller. Ranges were varied from 5- to 30-m distant from the receiver placed atop the second level of the receiver scaffold. The range increment was 5 m. Samples were collected from the SPL at the rate of 20 Hz.

5.1.1 Developmental Power versus Range Measurement Series at 19472 (March/April 2009)

An initial series of range vs. power measurements were performed in the spring of 2009 involved the setup of an ultrasonic source emitter and a receiver plus associated computer control devices using parabolic dishes on both the emitter and receiver sides. The object was to propagate ultrasonic signals under different atmospheric conditions and varying the frequency to study the effects of the atmosphere on the propagated signal. In addition to the ultrasonic units, a sonic anemometer on a 2-m mast was positioned alongside the acoustic pathway to characterize the wind conditions present. This unit is also connected to the LabView laptop, but data were

collected using a stand-alone data acquisition program written for LabVIEW. Typical measurements consist of 1-min collections of data from the sonic anemometer and the SPL meter for a specified frequency of the emitter, and a specific range between emitter and receiver.

Unfortunately, this first series experienced further difficulties, even though the multipathing issue was believed resolved by positioning the receiver device atop the 19472 compound's scaffold. Following data collection it was believed that variations in the detected sonic levels could be averaged out over the complete time record of each data set. However, upon performing that averaging and analyzing the results, in attempting to correlate results obtained at different frequencies and at different ranges an inconsistent pattern of signal losses arose.

Figures 21–24 intercompare sound data collected at 5-, 10-, 15-, and 20-m downrange, for various frequencies, on March 19, 2009.

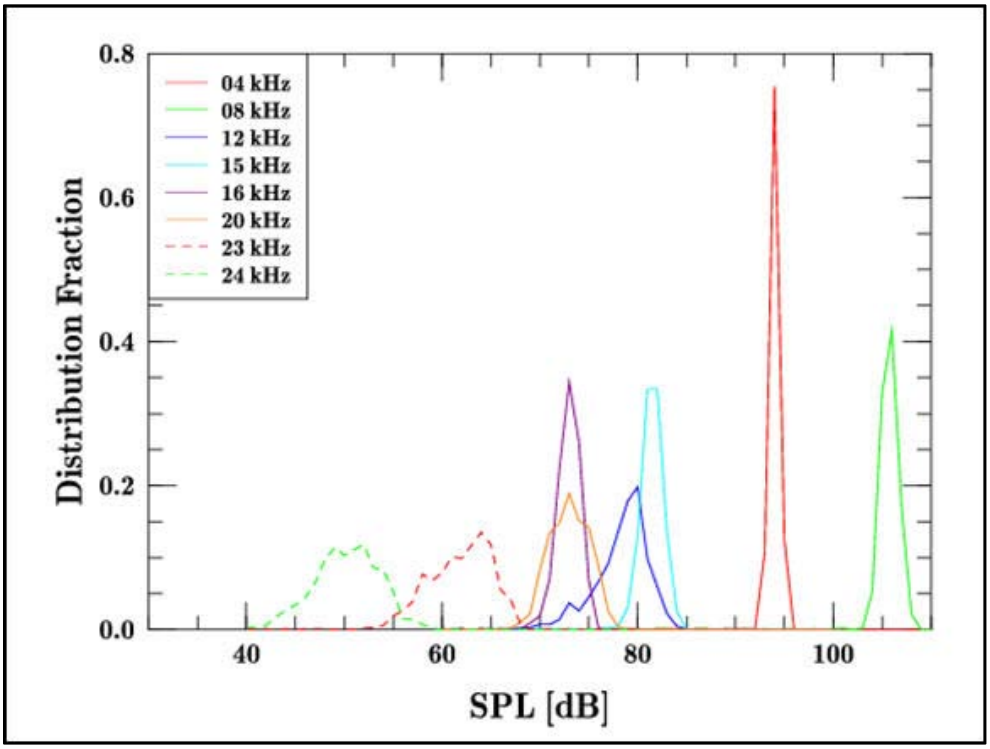

Figure 21. 5-m sound pressure distribution data for various frequencies.

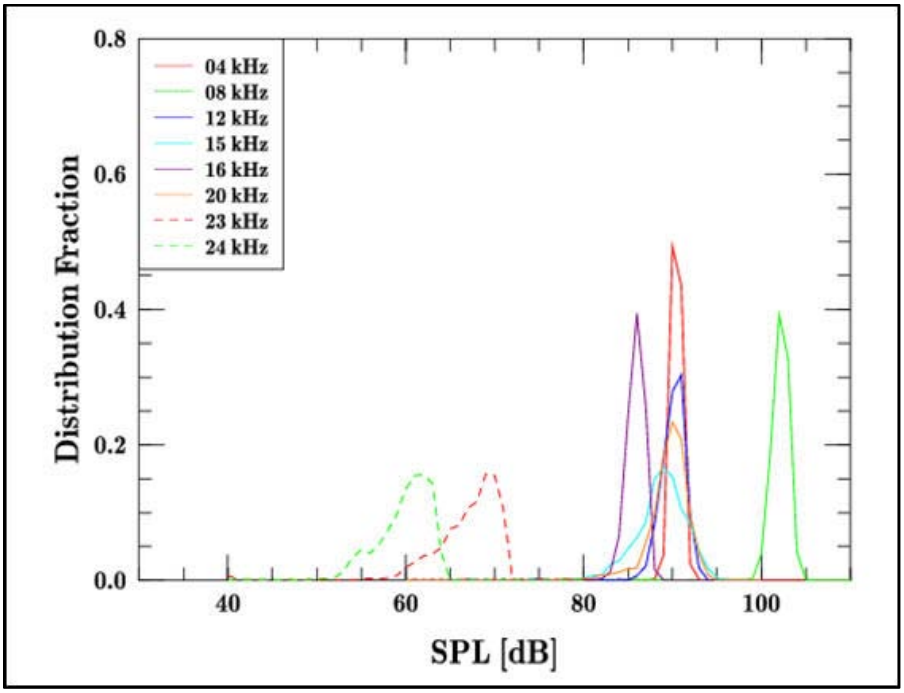

Figure 22. 10-m sound pressure distribution data for various frequencies.

As an example of the difficulties noticed, while both the 4- and 8-kHz signals appeared to shift downward in energy by approximately the same amount (roughly 4 dB between 5 and 10 m), the amount of the shift expected should have been 6 dB associated with the energy loss with a path length doubling (the $1/r^2$ effect). In contrast, the remaining signals all appear to increase in strength from 5 to 10 m! Yet, perhaps (it was argued) either the 5- or 10-m readings were somehow anomalous. It was hoped that the 15- and 20-m readings would make sense of the previous ambiguities. Based on this premise, we considered the remaining plots.

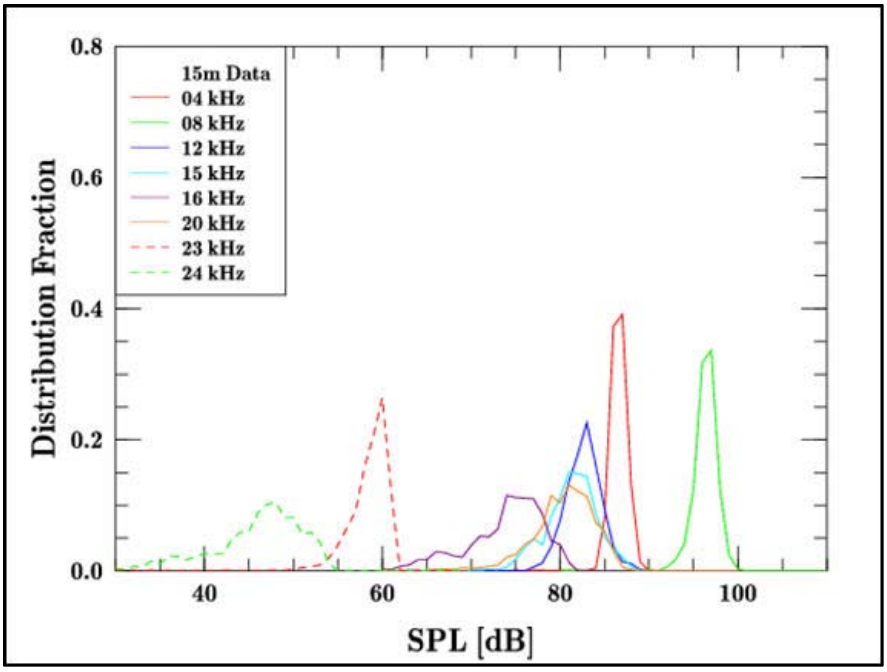

Figure 23. 15-m sound pressure distribution data for various frequencies.

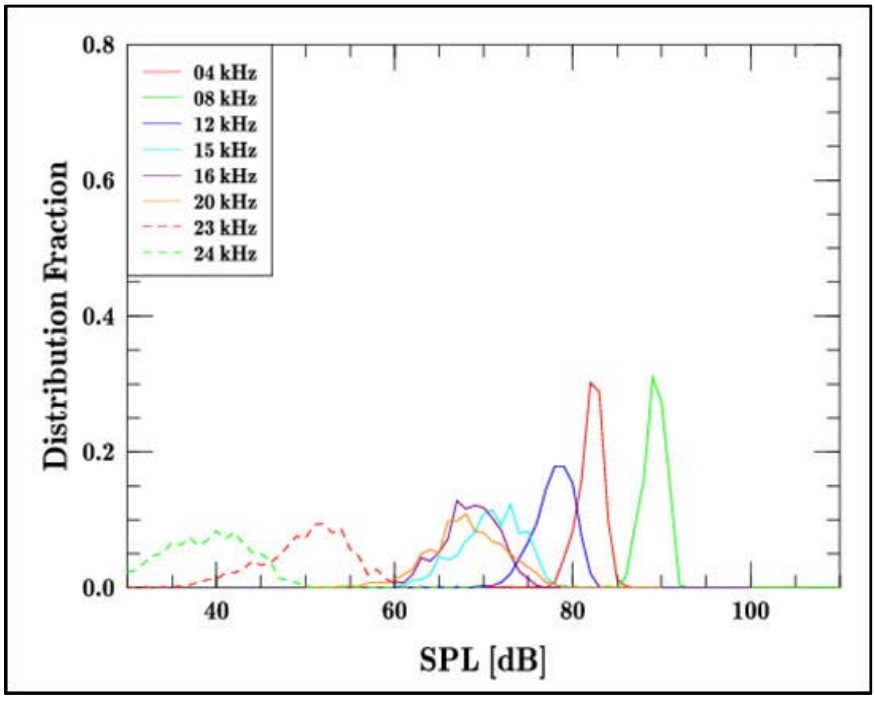

Figure 24. 20-m sound pressure distribution data for various frequencies.

In considering these remaining plots, one constant appeared to be the relative shift between the 23- and 24-kHz distribution patterns. They appear shifted by approximately 12 dB in each case. However, being in close proximity spectrally, we expect these two to behave similarly.

For a less consistent pair, the 16- and 20-kHz distributions are roughly identical at 5 and 20 m, yet the 20-kHz signal exhibited a stronger peak response at 10 and 15 m. One possible explanation was that perhaps atmospheric scattering could account for these variations. Yet, if atmospheric variations were cause the means to drop anomalously, then there should be some corresponding change in the width of the distribution functions, and these did not appear to be correlated.

The alternative possibility postulated was that during these measurements rather strong cross winds were present. It was hypothesized that the wind effects could be causing the beam generated by the parabolic dish to be pushed off the center of the receiver aperture or tilted, resulting in a varying focusing point of the sonic energy in the receiver dish. An alternative explanation was that possibly the parabolic dish was producing a lobe structure of the beam at different frequencies emerging from the emitter that would produce varying results depending on small angular changes in the directions of either the emitter or receiver dishes.

By either reckoning it was believed that the parabolic dishes were a liability to the measurements. Therefore, it was decided that the dishes would be replaced on both ends of the acoustic path. On the transmitter side the dish was replaced by the rectangular horn. This combination featured the widest angle beam, producing (it was hoped) the least possible lobe structure or possibility for the beam to be blown off the receiver. On the receiver side, it was decided that the receiver would be used in an unaugmented fashion. Estimates of the decibel loss associated with this step were believed to be approximately 14 dB at most, and since the power of the initial signal was at greater than 90 dB in most cases, this loss was considered acceptable.

However, prior to the restart of testing, our experimental operations were shut down due to an ARL safety stand-down. Prior to restarting, safety procedures in place had to be documented and approved, as discussed in section 3. While this process was occurring, funding arrived, and the set of rectangular, round, and trumpet horns was purchased that would permit a wider array of beam propagation options. Also, the testing software was augmented to permit the acoustic and sonic anemometer data sets to be collected in a time-tagged manner and merged into a single output file, and a data communications package (transmit and receive) was developed in LabVIEW. The road leading to the site was also paved (see figure 25).

Figure 25. View down “test range” road leading to the 19472 site.

5.1.2 Refined Power versus Range Measurement Series at 19472 (October/November 2009)

Once safety concerns had been addressed, new software had been written, and new equipment integrated into our data acquisition methodology, a follow-on series of measurements were scheduled in mid-October to again study the range versus power problem considered in the spring. The main propagation path lay down the road leading out of the site (figures 6 and 25). The receiver SPL meter was placed at the 12-ft level of the scaffold (figure 7) and the rectangular horn was used to propagate the beam so that a wide angle beam would be presented at the receiver, but the narrow vertical dispersion would avoid ground reflections of the beam.

For these measurements the 15- and 23-kHz measurement frequencies were dropped, but the range was extended to 30 m, again in 5-m increments. An initial series of measurements were taken in October and analyzed. These results are shown in figure 26 as colored balls. The results plotted have been normalized such that each trace of sound level (propagated power) versus range reads 100 at 5-m range.

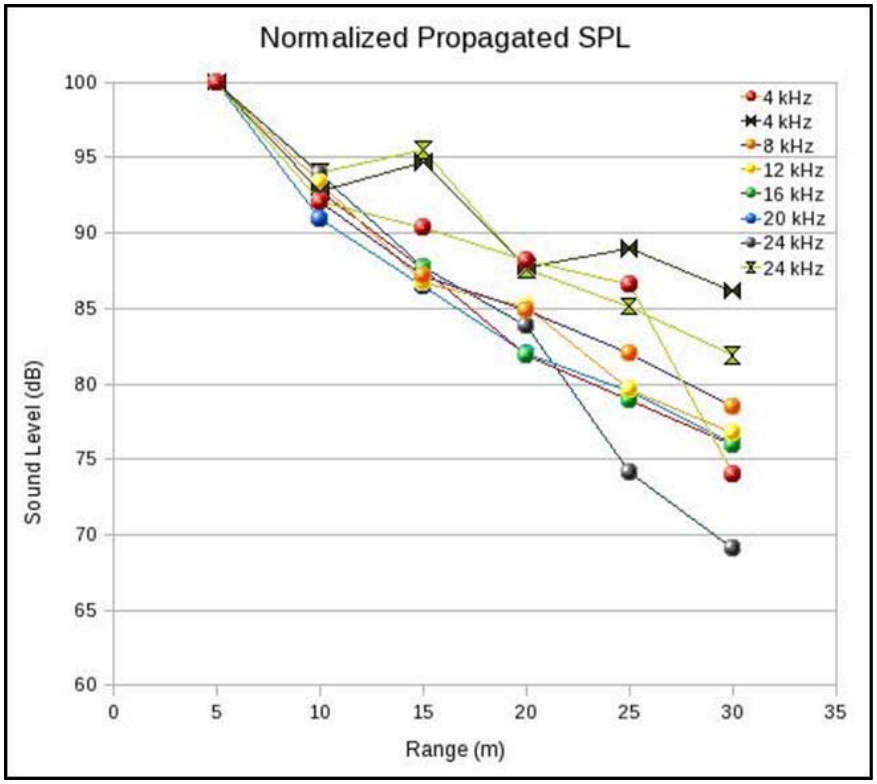

Figure 26. Range versus propagated SPL power for varying wavelengths.

This series of measurements appears to be somewhat improved over the prior results, yet there does not appear to be a significant difference in propagated power as a function of range for frequencies between 8 and 20 kHz. Nevertheless, there do appear to be the same type (though perhaps not to the same degree) of cross-overs between different frequency results.

The one trend that does perhaps indicate a frequency shift effect can be seen in the 8-kHz line. It does appear to separate somewhat (by 3–4 dB) from the higher frequency results, particularly at 30 m. Similarly, the 4-kHz results also appeared to diverge, but only at ranges through 25 m. The 30-m result appeared as an outlier. On the other hand, the 24-kHz results appeared to behave approximately similar to lower frequency results through 20 m, but then seemed to diverge low for the 25- and 30-m readings.

Because of these anomalous behaviors, we felt that further measurements of the 4- and 24-kHz frequencies might be in order. In the original sets taken in October the emitter was repositioned at a given range from the receiver scaffold and all six frequencies were tested in turn. It was thought that perhaps due to the presence of varying wind conditions it would be more consistent to attempt a series of measurements involving repositioning of the emitter to different ranges while only testing one frequency at a time. In this way the wind conditions would presumably remain relatively constant for each frequency. It was decided to only test the two outlier frequencies. These results are shown in the figure as bowtie markings.

Unfortunately, these seemed to exhibit as many odd behaviors in the second series of measurements as during the first. The 15-m data sets were particularly intriguing in that the resulting power levels increased for both frequencies by nearly the same amount.

We conclude from these results that we were detecting significant amounts of acoustic scattering, even at short range. We may also note that the $1/r^2$ effect is clearly present. According to this rule we would expect the doubling in path length between 5 and 10 m to produce a 6-dB loss from 100 to 94 dB. This is observed. Similarly, this rule would indicate a drop to 88 dB at 20 m. This also was observed, however we must view the two November results at 15 m as anomalous. Likewise, we would expect at least another 3.5-dB drop between 20 and 30 m, and there again the November 4-kHz result appears anomalous, but the remaining results appear consistent. In most cases, however, the drop between 20 and 30 m appears to be on the order of 5 dB or greater. This would be consistent with increased signal losses due to molecular attenuation and atmospheric turbulence scattering losses.

5.2 Ultrasonic Acoustic Communications Proof of Concept Tests (November 2009)

A repeat of acoustic propagation experiments at 4 and 24 kHz this week at the Wideband Acoustic Technology and CHaracterization Experimental Range (WATCHER) at building 19472 confirmed that variations in the propagated power levels are likely due to atmospheric turbulence scattering the acoustic energy out of the main propagation pathway. Various statistical analysis methods are being considered to characterize the distribution of these effects of turbulence on sound intensities at different frequencies with range.

6. Feasibility Analysis Results

Once a pair of functional ultrasonic communications systems had been constructed (an AM version and an FM version), these systems were tested at the building 19472 compound. The first tests occurred indoors and consisted of propagating a series of bit-encoded characters across a single room. Both modulation schemes employed a transmitter with an attached rectangular horn that sent data to a receiver consisting of a single high sensitivity flat-spectral-response microphone.

The first approach to be tested was the AM communications scheme. This approach was rejected almost immediately because its modulation frequency could be audibly detected, a property that is at odds with the intended reduction in observability for the intended ultrasonic application.

A FSK modulated FM system was then tested. Although it did not generate as high an audible signature level as the AM modulation approach, the performance of this initial configuration for FM modulation was still disappointing in that respect. Frequently, the transitions between the

"0" signal frequency to the "1" signal frequency did produce audible clicks in our first tests. This phenomenon was determined to be due to a combination of the frequencies chosen, the duration of each bit-state signal, and a lack of suitable tapering of the single-frequency signal envelope.

Despite these limitations, indoor tests showed that the FSK system was capable of communicating at a rate of 300 baud (bits per second) or more, as long as multipathing influences were not present. However, when the orientation of the emitter was changed so that it did not directly face the microphone, significant multipathing effects were observed due to wall reflections. When multiple wall reflection path signals were added to the transmitted signal an obvious degradation in data transmission reliability ensued. The explanation for observed multipathing problems is easily demonstrated with the aid of the schematic illustration of figure 27.

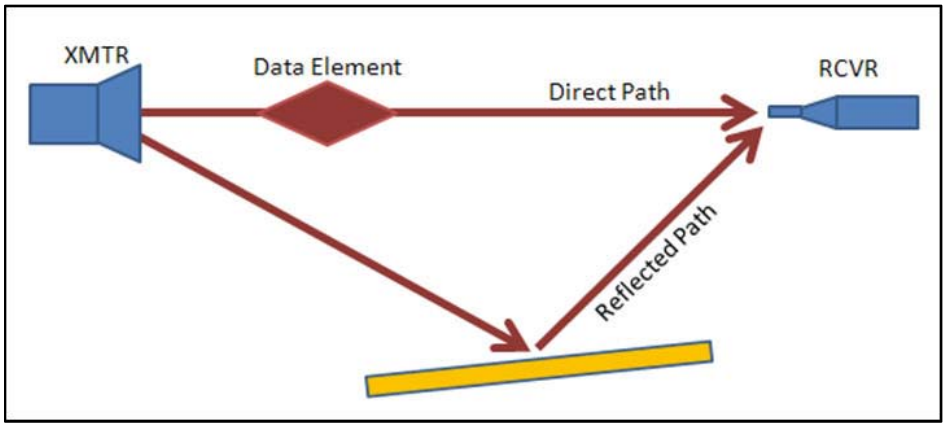

Figure 27. Multipathing bit error geometry.

The impact of multipath distortion upon data transfer for our proof of concept system may be illustrated as follows. The emitter generates a single frequency signal pulse representing either a zero (20 kHz) or a one (25 kHz) tone. At the nominal speed of sound (approximately 340 m/s) and a 300-baud data transmission rate, each signal 'bit' pulse will have a physical length of approximately 1 m. This effect is illustrated in figure 27 by the red "Data Element" diamond. Since the direct path will also be the shortest path, this data packet will travel fastest to the receiver by the direct route. The alternative "Reflected Path" will take longer to traverse, but eventually the reflected signal will also reach the receiver aperture. Thus, if there is a sequence of data packages travelling along both the direct and reflected routes, and if the lengths of the two respective paths differ by more than the length of a single data packet, then the reflected signal of a previous packet may be received during reception the direct signal for a given packet. In this case, the system might need to invoke specialized techniques to be able to discriminate between the most direct path result and that of the time shifted reflected path result.

It might still be possible to discriminate between the direct and reflected signals, particularly if the direct signal is significantly stronger than the reflected signal. This would be an application of "Rician" statistics, in which the main signal is much stronger than multiply reflected signals. This is illustrated by figure 28, which depicts a 300-baud, 3-bit FSK "101" signal combined with two delayed and attenuated reflections of itself. It is apparent that the direct signal has some margin above the multipath "noise", but the margin is much reduced when reflections coincide in time and sum to a larger power level. On the other hand, in an extreme case there may not be any clear direct signal. In this instance, the received signal might consist of only a summation of multiple reflected signals. This case is characterized by "Rayleigh" statistics similar to that of a random walk experiment. Figure 29 shows the same scenario as that of figure 28, but with the direct path signal absent. The integrity of the 3-bit signal is clearly in doubt, as the noise margin is practically non-existent. In such cases advanced methods would need to be employed to avoid inter-symbol interference.

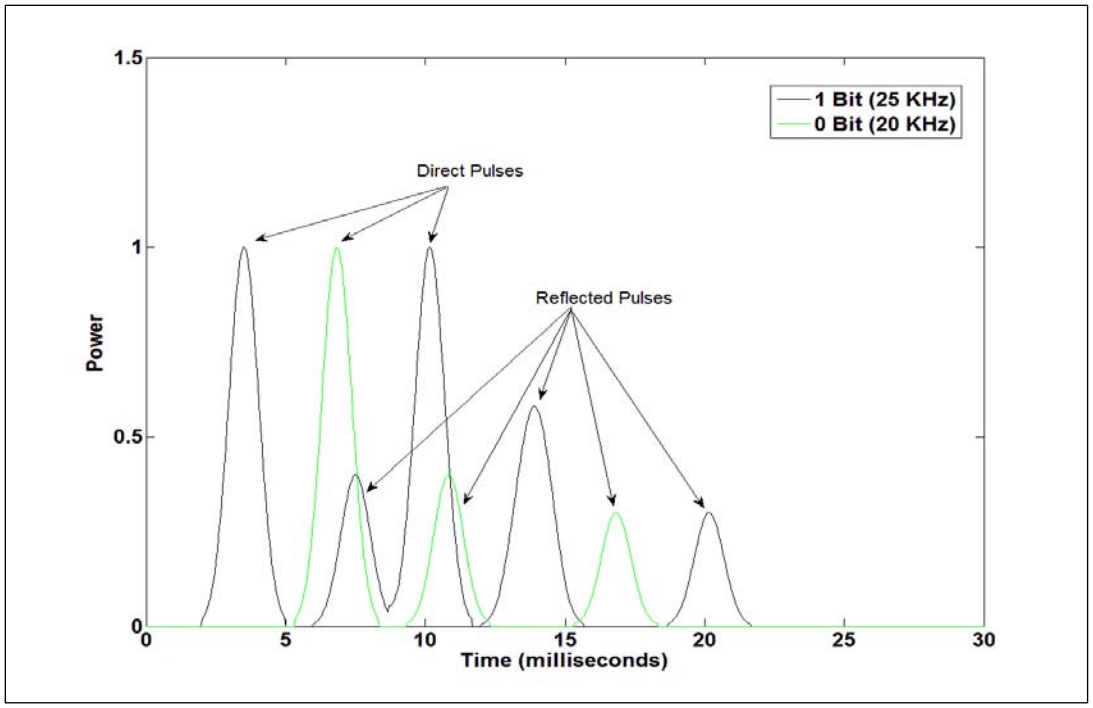

Figure 28. Illustration of strong direct signal in the presence of weaker reflected (multipath) signals.

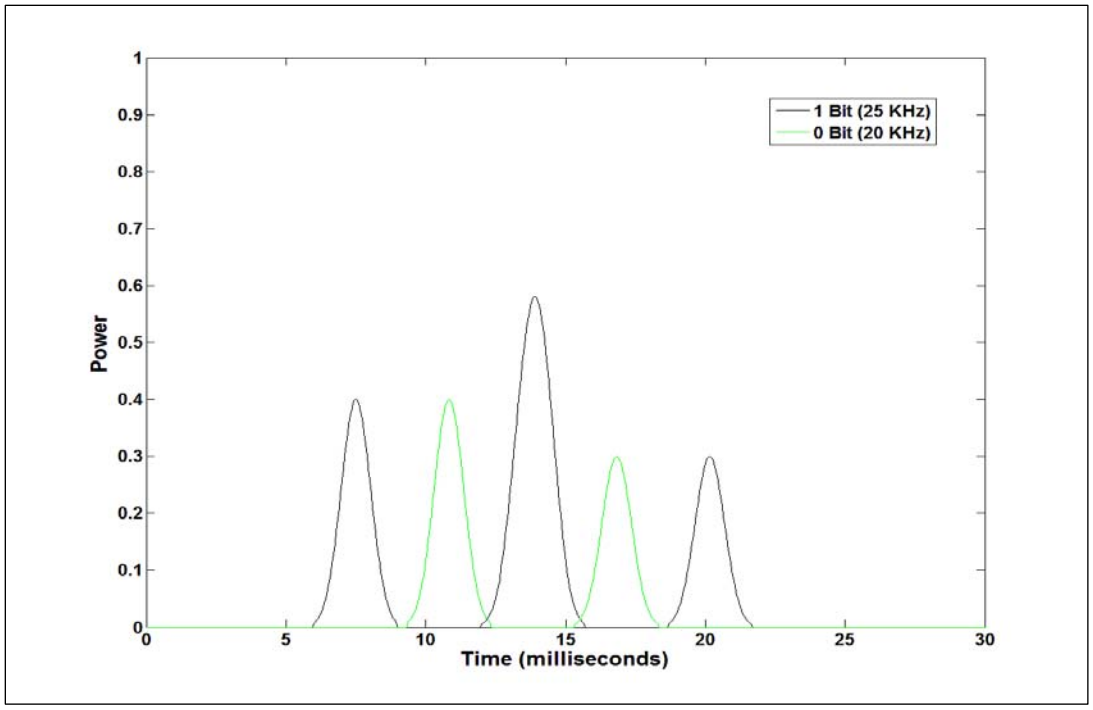

Figure 29. Illustration of reflected (multipath) signal in the absence of a direct signal.

However, not all ultrasonic applications would need to pass high bit-rate data. There are some data messages that are significant with even just a few bytes or even a few bits of data. In such cases, the baud rate necessary is less important because the significance of individual bits is higher. A prime example for such an application of this technology is the implementation of an Identification Friend-or-Foe (IFF) signal system for dismounted infantry in an urban setting. For this case the baud rate could be lowered to the level where only a single frequency tone pulse would be detectable at any time within the sphere reachable by a given emitter. The size of this sphere (and thus the maximum allowable bit rate) would be defined by the receiver sensitivity and the strong range dependent signal losses inherent to ultrasonic sources.

Assuming that an ultrasonic signal cannot be detected beyond approximately 70 m in any one direction, the baud rate could be lowered to 5 bits per second, allowing approximately enough data to transmit to identify one letter per second.

We modified the initial FM system to reduce the baud rate to eight samples per second and found that the system could propagate around corners fairly easily given a suitable reflecting surface. The system also appeared to be relatively immune to multipathing effects over short ranges, though further testing is necessary to determine the exact extent of the modified system's capabilities.

In addition to the reduction in baud rate, the emitter system was also modified to add a relatively simple sine-wave signal envelope designed such that for each data bit at a single frequency, the

sine envelope varied over the range zero to pi. This taper of the signal envelope made the emitter inaudible to human hearing.

7. Conclusions

This report provides an initial overview of the potential for short range ultrasonic acoustic communications within the atmosphere. The applications examined here are of direct interest to the Army because they have potential to benefit the operational safety and combat effectiveness of the Soldier. In order to realize these benefits for the Soldier, one must attempt to unify various disparate elements based on available theory, experimental data, and past engineering results into specific engineering concepts. We have accomplished several stages of this process by reviewing past experimental and theoretical investigations on boundary layer atmospheric ultrasonic propagation, establishing an infrastructure for outdoor testing, formulating software control for several applications, and performing model analysis of ultrasonic proof-of-concept systems. Specifically, we have achieved the following milestones:

1. A literature survey of prior art in the application of ultrasonic systems in the atmospheric environment has been made (and is continuing).
2. A semi-empirical model for the ultrasonic propagation environment has been implemented from information available in the literature.
3. Preliminary experiments have produced results that are in reasonable agreement with these models.
4. A physical infrastructure and framework (in the form of the WATCHER facility) has been constructed.
5. A software virtual instrument framework based on the LabVIEW package has been developed and tested for ultrasonic sources, detectors, and analytical devices.
6. Using this infrastructure, more detailed experiments have characterized angular emission properties of sources and their propagation performance.
7. The LabVIEW framework has been used to create and test a low data rate proof-of-concept communication system.

While our initial experimental efforts have produced a few anomalies in the observed propagation data, they do correspond reasonably well with model results in general. It is clear from our model results that a comprehensive suite of meteorological support sensors will be necessary in order to better characterize the ultrasonic propagation environment. In particular, better characterization of the turbulence levels (through analysis of time series of sonic anemometer data or optical scintillometer data), outer scales of turbulence (through application

of similarity techniques), and humidity (from local hygrometer measurements) should provide a better fit with model results and higher confidence in the characterization of the propagation environment.

Our experimental results for low speed data transmission using FSK modulation of an ultrasonic carrier indicate considerable promise for urban warfare IFF applications at the squad level. It has been suggested that spread-spectrum modulation methods that are commonly employed for acoustic communication in the submarine environment may also improve the data rate to the point that other atmospheric ultrasonic communications concepts could become feasible. Spread-spectrum techniques may also prove useful for short range, near-surface atmospheric sounding applications for ultrasonic systems.

We hope to extend our activity and results to help us develop and explore other ultrasonic applications that might be of interest and utility to the Army.

8. References

Akerman, A. M.; Ayers, C. W.; Haynes, H. D. Ultrasonic Speech Translator and Communication System. U.S. Patent 5,539,705, July 23, 1996.

Baikalova, R. A.; Krekov, G. M.; Shamanaeva, L. C. Theoretical Estimates of Sound Scattering by Atmospheric Turbulence. *J. Acoust. Soc. Am.* **1988**, *83*, 1332–1335.

Bradley, S.; Webb, T. *Use of an Ultrasonic Sodar to Sense Raindrop Size Distribution*, Physics Department, University of Auckland, Auckland, New Zealand (2001).

Busnel, R.G.; Classe, A. *Whistled Languages*, Springer-Verlag: New York; 1976.

Cogan, J.; Measure, E.; Wolfe, D. *Atmospheric Soundings in Near-Real Time from Combined Satellite and Ground-Based Remotely Sensed Data*; ARL-TR-1481; U.S. Army Research Laboratory: White Sands Missile Range, NM, 1997.

Desart, E. *Sound absorption by air as per ISO 9613-1, Mar 11, 2004.* Acoustic Forum. http://forum.studiotips.com/viewtopic.php?t=158 (accessed April 2010).

Haynes, H. D.; Akerman, M. A.; Baylor, V. M. *Final Report: Ultrasonic Communication Project, Phase 1, FY 1999*, Report Y/NSP-252, National Security Program Office, Oak Ridge Y-12 Plant: Oak Ridge, TN, 2000.

Heard, M. C. Short range communications using modulated ultrasound. *IEE Colloquium* (Digest) **1983**, 2.1–2.3.

Holm, S. Airborne Ultrasound Data Communications: The Core of an Indoor Positioning System. *Proc. IEEE Ultrasonics Symposium;* Rotterdam, the Netherlands, 2005; Vol 3, pp 1801–1804.

Hummel, J. R., Ed. *High Energy Laser Propagation Handbook, Volume II, HEL System Test Facility Atmospheric Characterization*; ASL-TR-0148; U.S. Army Atmospheric Sciences Laboratory: WSMR, NM, 1984.

Ishimaru, A. *Wave Propagation and Scattering in Random Media, Volume 2, Multiple Scattering, Turbulence, Rough Surfaces, and Remote Sensing*; Academic Press: New York, 1978.

ISO 9612-1:1993, Acoustics–Attenuation of Sound during Propagation Outdoors.

Kaye and Laby. *Tables of Physical and Chemical Constants, National Physical Laboratory: UK, 2009*. http://www.kayelaby.npl.co.uk/general_physics/2_4/2_4_1.html (accessed April 2010).

Li, C.; Hutchins, D. A.; Green, R. J. Short-Range Ultrasonic Digital Communications in Air. *IEEE Trans Ultrason Ferroelectr Freq Control* **2008**, *55*, 908–918.

Neff, W. D. *Quantitative Evaluation of Acoustic Echoes from the Planetary Boundary Layer*. NOAA Technical Report ERL322-WPL: Boulder, CO, 1975.

Shamanaeva, L. G. The Dependence of Sound Extinction on the Parameters of Thermal Turbulence in the Atmospheric Boundary Layer. *J. Acoust. Soc. Am.* **1983**, *73*, 780–784.

Shamanaeva, L. G.; Burkatovskaya, Yu. B. Statistical Estimates of the Contribution of Multiply Scattered Radiation to the Intensity of Acoustic Radiation Transmitted Through a Lower 500-m Atmospheric Layer. *Russ Phys J.* **2004**, *47* (12).

Shannon, C. E. A Mathematical Theory of Communication. *The Bell System Technical Journal* **1948**, *27*, 379–423 and 623–656.

Stull, R. B. *An Introduction to Boundary Layer Meteorology*, Kluwer Academic Publishers: Dordrecht, The Netherlands, 1988.

Sutherland, L. C., Ed. *Sonic and Vibration Environments for Ground Facilities–A Design Manual*; Contractor Report WR 68-2; Wyle Laboratories: Huntsville, AL, 1968.

Zurek, R. A.; Charlier, M. L.; Dietrich, A. Omnidirectional Ultrasonic Communication System. U.S. Patent 6,363,139, March 26, 2002.

Appendix. Ultrasonic Measurements Safety Standard Operating Procedure

The following attachment was drafted and approved by ARL.

Standard Operating Procedure for
Ultrasonic Sensing Propagation Measurements at Bldg. 19472, WSMR, NM
(Last Revision: August 17th, 2009)

1. Purpose: This standard operating procedure (SOP) documents potential hazards during ultrasonic propagation testing at WSMR bldg. 19472, and addresses engineering and administrative controls to be implemented to mitigate these potential hazards.

2. Scope: This SOP applies to personnel engaged in ultrasonic measurements at bldg. 19472, as well as other personnel visiting the site during testing operations.

3. General: Ultrasonic measurements at building 19472 consist of a laptop computer connected via National Instruments software and modules to an amplifier that powers an ultrasonic emitter. The 19472 building compound is located in a desert area approximately 3 miles south of the main post area. The map below shows a satellite image of the 19472 building compound (center) and its environs including the nearest adjacent WSMR building compound, the 500K site, nearly 400 meters away.

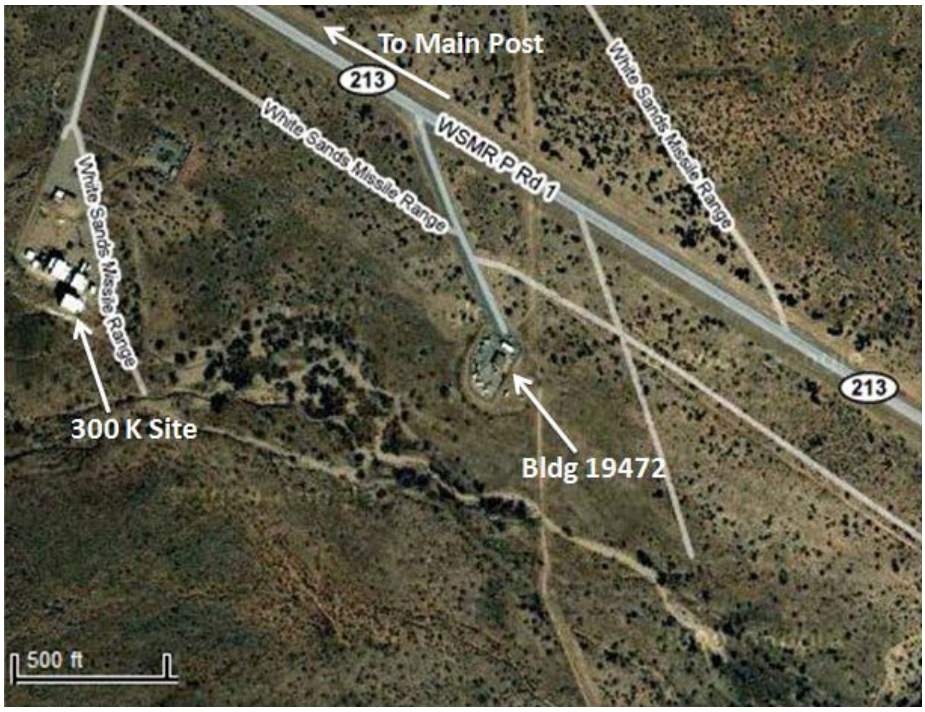

Building 19472 Compound.

Signals generated by the ultrasonic emitter are propagated through air via either a direct emission (basically omni-directional) or through a focused propagation using a 12-inch parabolic dish. Signals generated are detected using a passive receiver device connected to a pre-amplifier that sends its

signals back to a laptop computer through National Instruments software and modules. Emitter and/or receiver devices **may** at times (or may not) be set up on the second level of a 12 ft. stairway scaffold located near the gate of the compound, depending on conditions being tested.

No deviations from this Standing Operating Procedure (SOP) will be permitted. Whenever the approved methods in this SOP must be changed, the SOP must first be revised and approved in writing by the ARL Safety Office.

4. Responsibilities:

a. Training Requirements: All test personnel shall receive electrical safety training prior to operating test equipment or participating in setup activities. Only test personnel who have received proper scaffold training, that includes fall arrest training, may mount, erect, assemble, or disassemble scaffold equipment on site.

b. The test director (senior test person on site) shall ensure that test personnel are operating in accordance with this SOP, and that site visitors are properly equipped with hearing protection during testing. The test director shall be cognizant of all personnel on site during testing and ensure that all are aware of when active sound generation events are occurring.

c. Supervisory personnel shall ensure that test personnel have been properly trained and equipped for testing operations at the site, as well as being properly instructed in the provisions of this SOP.

5. Personnel Limits: Only authorized and trained personnel shall operate electronic, emitter, and receiver test equipment. Only authorized and trained personnel shall mount scaffolding equipment. Visitors to the site shall be escorted during testing operations and shall be supplied with appropriate hearing protection by test personnel.

6. Material Limits: All electronic devices will be operated within their design specifications. Scaffolding equipment will not be loaded beyond its design limitations.

7. Safety Requirements:

a. Engineering controls: The scaffolding available at the bldg. 19472 compound will consist of an Upright 12 ft. framed stairway scaffold. This scaffold is mounted with toe-guards at both the 6 ft. landing and the 12 ft. walkway. The width of this scaffold is 4 ft., such that the height-to-width ratio is 3-to-1, which exceeds the OSHA 4-to-1 standard for free standing scaffolding. The scaffold is secured to the bldg. 19472 perimeter fencing to provide additional stability. The scaffold has also been equipped with additional hand railings and cross bars at appropriate heights to provide additional support points and to assure that accidental fall hazard risk from the scaffold is minimized. The scaffold has two horizontal platform levels at 6 feet and 12 feet above ground with sections of stairs connecting each level. Cross railings surround each platform level at appropriate heights to protect personnel from accidental falls off the scaffold. While instrumentation will be securely emplaced on the 12 foot platform from below, at no time will personnel climb completely up and place their feet to crouch or stand on the 12 foot platform level.

All electrical equipment used for testing is UL approved.

b. Administrative controls:
A copy of this SOP will be posted at the 19472 building site at all times.

Test personnel must read and understand this SOP, as well as sign the SOP signature page, prior to participating in testing activities.

Site Activity: Ultrasonic testing operations at the bldg. 19472 site can be performed Monday through Friday from 6:00am to 6:00 pm. Approval must be obtained from the safety office to work outside normal working hours. All testing will be attended by trained users and a test director. At least two personnel must be on site whenever testing is underway. No unattended testing will be permitted.

User Training: All test personnel must have completed appropriate ARL R&D Electrical safety training, including electrical safety in field testing environments, prior to operating or setting up electrical equipment. Personnel erecting, disassembling, and mounting the stairway scaffold on site must have received prior OSHA scaffold training that includes fall arrest training.

Desert Operations: All personnel must be familiarized with operations in desert environments. Hats, sunscreen, and shade will be used during hot conditions to avoid heat injuries. Water will be maintained in the 19472 refrigerator. Operations at the site are only authorized if environmental conditions within the building are suitable to mitigate weather conditions present during the measurement operations.

Inclement Weather: The ultrasonic measurement equipment will not be operated under inclement weather conditions, to include storms, lightning, or high wind events in the vicinity of the 19472 building compound.

Electrical: In addition to other safety requirements, the following procedures shall be observed.

Analysis: Active test measurements may use (at times) a power amplifier to boost the ultrasonic acoustic emission. The power amplifier has the following specifications. Its maximum power output is 200 W. It can be operated in one of two modes, either bridged or un-bridged. In un-bridged mode the output is 0-40 V. In bridged mode the output is -40 -- +40 V for an RMS output voltage of 28 V. The maximum current is 15 Amps, but is further restricted such that the maximum output power is no greater than 200 W. When in use, the most likely mode to be used will be the bridged configuration to ensure that any signal modulation will carry a zero amplitude low frequency component. This will avoid low frequency noise components in the sound output.

Electrical Hazard Mitigation Procedures:

1. Laboratory measurement devices must be properly grounded and equipped with a primary on/off electrical power switch to enable operation. This power on/off switch should be placed in the off configuration when the devices are not intended to be used, and anytime during setup or breakdown of the system.

2. Inspect power cables for cuts or gaps in the covering over conductive wires. All equipment used should be UL listed. Verify UL listing. If a cable is not properly covered do not attempt to use.

3. Covers should never be removed from amplifiers or pre-amplifiers.

4. Outdoor facility power may only be used if a proper UL approved GFI (Ground Fault Interruption) device is in place.

5. All electrical equipment will be operated within its design parameters.

Noise: Noise will be controlled and/or hearing protection will be used to avoid noise hazards in accordance with OSHA guidance on ultrasonic sound sources found at http://www.osha.gov/dts/osta/otm/noise/health_effects/ultrasonics.html . According to the OSHA noise standard 1910.95, table G-16 (copied here) provides data on general noise Threshold Level Values in two categories: Ceiling Values, and 8-hour Total Weighted Average (TWA) exposures. No experimentation will exceed these thresholds.

Analysis: To provide more specific information, the conditions of testing are considered here in more detail. The emitter device being used in this testing generates 92 dB when driven by 1 Watt of power. This emitter is electrically equivalent to a 0.13 μF (micro-Farad) capacitor. Emitter equipment: Our primary emitter is electrically equivalent to a 0.13 μF capacitor. While the power supply is rated up to 200 W, the voltage output will be restricted to 50 V RMS based on the training of the operators. Frequencies emitted will also be limited to less than 25 kHz. At 25 kHz the emitter impedance reaches a minimum value of 49 Ω. This will mean the amplifier is supplying ~50 Watts of RMS power, a 17 dB power increase over the 1 W power level. This represents a maximum power level. At frequencies less than 25 kHz the power supplied is less.

TLVs® for Ultrasound			
	One-third Octave-Band Level		
	Measured in Air in dB re: 20 μ Pa; Head in Air		Measured in Water in dB re: 1 μ Pa; Head in Water
Mid-Frequency of Third-Octave Band (kHz)	Ceiling Values	8-Hour TWA	Ceiling Values
10	105[A]	88[A]	167
12.5	105[A]	89[A]	167
16	105[A]	92[A]	167
20	105[A]	94[A]	167
25	110[B]	--	172
31.5	115[B]	--	177
40	115[B]	--	177
50	115[B]	--	177
63	115[B]	--	177
80	115[B]	--	177
100	115[B]	--	177

The gain on the parabolic reflector used has been estimated based on a beam measured as 15 meters in radius at 75 meters in range. Assuming an otherwise hemispheric Lambertian sound source without the reflector, the reflector gain factor is 14 dB. Combining the initial 1 W noise power level plus the amplifier gain factor, and the reflector gain, the maximum sound level at 1 meter from the emitter's reflector exit aperture is 92+17+14 = 123 dB. For each doubling of range from the reflector beyond 1 m, since sound levels decrease using a power formula, the

sound level drops 6 dB. At 10 meters the maximum sound level is reduced to 105 dB, the ceiling level indicated in the above table. Therefore, for active tests, assuming the highest output power level as a worst case for a safety envelope calculation, we will employ barricades at 10 meters from the emitter and employ sound protection within this 10 meter zone. We will otherwise keep test and visitor personnel safely clear of emitting sources during testing. Hearing protectors rated at 29 dB have been procured and should be sufficient to reduce the maximum 123 dB to 94 dB to mitigate noise hazards under all conditions.

Conversely, when operating outside the cone of the reflector-focused sound energy, one might expect the maximum sound level to be 92+17-14 = 95 dB, a level within tolerance for short exposures, and a level of only 77 dB for ranges beyond 10 meters, below the hazard threshold. The primary hazard zone is thus in the forward direction when using the parabolic reflector.

When operating without the parabolic reflector the hazard is reduced to a maximum of 109 dB, but is omni-directional. For distances beyond 10 meters, this reduces to 91 dB, which can accept an exposure up to 3 hours per day, A-weighted.

Noise Mitigation Procedures:

1. All personnel on site will be equipped with hearing protection equipment during operations. All personnel will wear hearing protection when an emitter is propagating if working within 10 meters of the emitter.
2. No hearing protection will be necessary when operating in a passive (listening) mode.

Personal Protective Equipment:

1. Personal protective equipment shall include appropriate shoes for mounting of scaffolding equipment and the use of a hard hat in the vicinity of the scaffold whenever equipment is being mounted onto the scaffold or is currently mounted on the scaffolding.

2. A head covering is required for outdoor testing when temperatures exceed 95 degrees Fahrenheit.

3. Hearing protection shall be used when sustained audible sound levels exceed 90 dB or when instantaneous sound levels exceed a 105 dB sound level.

Scaffolding: Only test personnel who have been trained in scaffold operations may use the scaffold. This testing is available on-line at:

http://www.oshacampusonline.com/construction-english/scaffolding.html

Personnel moving emitter and receiver equipment to the mounting platform at 12 ft. shall work in tandem by passing the equipment up the tower rather than attempt to carry it up the stairs singlehanded. Proper footwear will be worn when working on the scaffold to provide non-slip footing. Handholds will also be used whenever possible. When moving about the scaffold when instruments are mounted on the scaffold, hard hats must be worn. When mounting equipment on the top platform of the tower, equipment should be secured to the scaffold. The scaffold will not be used under wind conditions exceeding 20 MPH. Personnel will not climb to, stand or crouch on the top level of the scaffold.

The scaffold will not be moved during testing. When positioned for mounting, the scaffold

wheels will always be locked.

1. Hazards to Avoid

a. Equipment will be operated for testing purposes. No other uses are authorized.
b. At no time will the covers be removed from system amplifier equipment.
c. At no time will electrical equipment be operated by untrained personnel.
d. At no time will the scaffold be mounted by untrained personnel.
e. At no time will visitors be permitted on site when testing is under way except with the approval of test personnel and supplied with appropriate hearing protection.
f. Personnel shall not climb to, stand or crouch on the top platform of the scaffold.

List of Symbols, Abbreviations, and Acronyms

°C	degrees Centigrade
AGL	above ground level
AM	Amplitude Modulation
ARL	U.S. Army Research Laboratory
ASCII	American Standard Code for Information Interchange
BED	Battlefield Environment Division
COTS	commercial off-the-shelf
DAQ	data acquisition
FM	Frequency Modulation
FSK	Frequency Shift Keyed or Frequency Shift Keying
IFF	Identification Friend-or-Foe
LabView	Laboratory Virtual Instrument Engineering Workbench
mB	millibars
met	meteorological
MMS	Meteorological Measuring Set
NI	National Instruments
RASS	Radio Acoustic Sounding System
RF	Radio Frequency
SODAR	Sonic Detection And Ranging
SOP	standard operating procedure
SPL	Sound Pressure Level
VI	virtual instruments
WATCHER	Wideband Acoustic Technology and CHaracterization Experimental Range
WSMR	White Sands Missile Range

No. of Copies	Organization
1 PDF	ADMNSTR DEFNS TECHL INFO CTR DTIC OCP 8725 JOHN J KINGMAN RD STE 0944 FT BELVOIR VA 22060-6218
3 HCs	US ARMY RSRCH LAB ATTN RDRL CIM P TECHL PUB ATTN RDRL CIM L TECHL LIB ATTN IMNE ALC HRR MAIL & RECORDS MGMT 2800 POWDER MILL ROAD ADELPHI MD 20783-1197
1 CD	US ARMY RSRCH LAB ATTN RDRL CIM G TECHL LIB APG MD 21005-5066
1 CD	US ARMY RSRCH LAB ATTN RDRL ROE N W BACH PO BOX 12211 RESEARCH TRIANGLE PARK NC 27009
1 CD	US ARMY RSRCH LAB ATTN RDRL CI J GOWENS 2800 POWDER MILL ROAD ADELPHI MD 20783-1197
1 CD	US ARMY RSRCH LAB ATTN RDRL CIE P CLARK 2800 POWDER MILL ROAD ADELPHI MD 20783-1197
1 CD	US ARMY RSRCH LAB ATTN RDRL CI R NAMBURU 2800 POWDER MILL ROAD ADELPHI MD 20783-1197
1 CD	US ARMY RSRCH LAB ATTN RDRL CI B SADLER 2800 POWDER MILL ROAD ADELPHI MD 20783-1197
1 CD	US ARMY RSRCH LAB ATTN RDRL CIE D D W HOOCK WSMR NM 88002-5501
2 CDS	US ARMY RSRCH LAB ATTN RDRL CIE D D TOFSTED WSMR NM 88002-5501
2 CDS	US ARMY RSRCH LAB ATTN RDRL CIE D S OBRIEN WSMR NM 88002-5501
2 CDS	US ARMY RSRCH LAB ATTN RDRL CIE D M S DARCY WSMR NM 88002-5501
1 CD	US ARMY RSRCH LAB ATTN RDRL CIE D D S ELLIOTT WSMR NM 88002-5501
1 CD	US ARMY RSRCH LAB ATTN RDRL CIE D E CREEGAN WSMR NM 88002-5501
2 CDS	UNITED STATES MILITARY ACADEMY COMBAT SIMULATION LAB P WEST WEST POINT NY 10996
Total:	21 (1 PDF, 3 HCs, 17 CDs)